Biophysical Reviews and Letters
Vol. 4, Nos. 1 & 2 (2009) 77–137


World Scientific
www.worldscientific.com

# ACTIVE BIO-SYSTEMS: FROM SINGLE MOTOR MOLECULES TO COOPERATIVE CARGO TRANSPORT

REINHARD LIPOWSKY*, JANINA BEEG, RUMIANA DIMOVA,
STEFAN KLUMPP†, STEFFEN LIEPELT,
MELANIE J. I. MÜLLER and ANGELO VALLERIANI

*Department of Theory & Bio-Systems,*
*MPI of Colloids and Interfaces‡*
*Science Park, 14424 Potsdam, Germany*
**reinhard.lipowsky@mpikg.mpg.de*

Received 9 October 2008

Living cells contain a large number of molecular motors that convert the chemical energy released from nucleotide hydrolysis into mechanical work. This review focusses on stepping motors that move along cytoskeletal filaments. The behavior of these motors involves three distinct nonequilibrium processes that cover a wide range of length and time scales: (i) Directed stepping of single motors bound to a filament; (ii) Composite motor walks of single motors consisting of directed stepping interrupted by diffusive motion; and (iii) Cooperative transport by teams of several motors. On the molecular scale, the energy conversion of these motors leads to single steps along the filaments with a step size of about 10 nm. The corresponding chemomechanical coupling is governed by several distinct motor cycles, which represent the dominant pathways for different values of nucleotide concentrations and load force. For the kinesin motor, the competition of two such cycles determines the stall force, at which the motor velocity vanishes and the motor reverses the direction of its motion. Because of thermal noise, the stepping motors unbind from the filaments after a certain run time and run length. For kinesin, the run time is about 1 s and the run length is about 1 $\mu$m for high ATP concentration and low load force. On length scales that are large compared to the run length, a single motor undergoes composite walks consisting of directed stepping interrupted by diffusive motion. The relative importance of bound and unbound motor states depends on the binding and unbinding rates of the motors. The effective transport velocity and diffusion coefficient of the motors are determined by the geometry of the compartments, in which the motors move. The effective diffusion coefficient can be enhanced by several orders of magnitude if the motors undergo active diffusion by interacting with certain filament patterns. In vivo, stepping motors are responsible for the transport of vesicles and other types of intracellular cargo particles that shuttle between the different cell compartments. This cargo transport is usually performed by teams of motors. If all motors belong to the same molecular species, the cooperative action of the motors leads to uni-directional transport with a strongly increased run length and to a characteristic force dependence of the velocity distributions. If two antagonistic species of motors pull

†Current address: Center for Theoretical Biological Physics and Department of Physics, UCSD, La Jolla, California 92093-0374, USA
‡URL: http://www.mpikg.mpg.de/th

on the cargo, they perform a stochastic tug-of-war, which is characterized by a subtle force balance between the two motor teams and leads to seven distinct patterns of uni- and bi-directional transport. So far, all experimental observations on bi-directional transport are consistent with such a tug-of-war. Finally, the traffic of interacting motors is also briefly discussed. Depending on their mutual interactions and the compartment geometry, the motors form various spatio-temporal patterns such as traffic jams, and undergo nonequilibrium phase transitions between such transport patterns.

*Keywords*: Molecular motors; nonequilibrium processes; chemomechanical coupling; force generation; composite motor walks; uni-directional transport; bi-directional transport; motor traffic.

## 1. Introduction

In each living cell, we find many different molecular motors and colloidal machines that perform various tasks[1] such as assembly and synthesis of macromolecules, ion transport through membranes, cargo transport along filaments, cell division, and cell locomotion. These motors and machines act as little 'demons' or 'nanorobots' that keep the living cell in a highly ordered state far from equilibrium. This self-organization is based on the energy conversion of the motors, which transform chemical energy into mechanical work.

In most cases, the molecular motor consists of a protein complex that interacts with another colloidal structure such as a macromolecule, membrane, or filament. Prominent examples are: (i) DNA and RNA polymerases, which move along the strands of DNA in order to replicate it and to transcribe it into RNA; (ii) ribosomes that attach to mRNA and translate the nucleotide sequence into proteins; (iii) membrane pumps, which transport ions and small molecules across membranes; (iv) myosins in muscles, which work in ensembles and collectively displace actin filaments; and (v) cytoskeletal motors, which bind to the filaments of the cytoskeleton and then walk along these filaments in a directed fashion.

In all of these examples, the motors are powered by the hydrolysis of adenosine triphosphate (ATP). Thus, these motors represent ATPases, i.e., catalysts or enzymes for the hydrolysis of ATP. This hydrolysis process consists of several substeps: first, ATP is cleaved into ADP/P, i.e., bound adenosine diphosphate (ADP) and inorganic phosphate (P), then the P is released from the motor, and finally the ADP is typically released as well. For the concentrations that prevail in living cells, the ATP hydrolysis is strongly exergonic or 'downhill' but it is also quite slow in the absence of any enzymatic activity. The motors act as enzymes for this chemical reaction which leads to much faster hydrolysis rates. In addition, these motors are also able to transform the chemical energy released from the ATP hydrolysis into useful work.

In this review, we will focus on cytoskeletal motors such as kinesin, see Fig. 1(a), that walk processively along cytoskeletal filaments in a directed manner and are essential for intracellular transport, cell division, and cell locomotion.[2–4] Three superfamilies of processive cytoskeletal motors have been identified: kinesins,

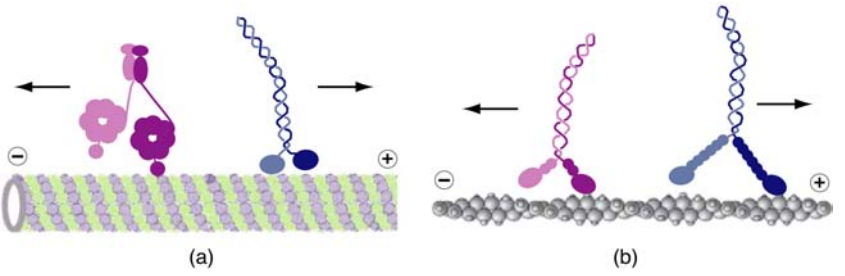


Fig. 1. Stepping motors: (a) Microtubule with one dynein (violet) and one kinesin (blue) motor. The filament consists of tubulin dimers that provide a lattice of binding sites with a lattice parameter of 8 nm. (b) Actin filament with one myosin VI (violet) and one myosin V (blue) motor. Both filaments are polar and have two different ends, a plus and a minus end. Each motor walks either towards the plus or the minus end as indicated.

dyneins and myosins.[4,5] Kinesins and dyneins bind to microtubules as shown in Fig. 1(a) whereas myosins bind to actin filaments as shown in Fig. 1(b).

The movements of cytoskeletal motors cover many length and time scales.[6,7] Already for a single motor, one can distinguish three dynamical regimes: the single-step dynamics of the motor protein which arises from the coupling of the molecular conformation to ATP hydrolysis; the directed walks of the motor along the filaments; and the composite walks of the motor as it repeatedly unbinds from and rebinds to the filaments.

The single-step regime covers all molecular processes up to a single mechanical step of the motor. Kinesin, for example, walks in a 'hand-over-hand' fashion, i.e., by alternating steps, in which one head moves forward while the other one remains bound to the filament.[8,9] Each step corresponds to a motor displacement of 8 nm corresponding to the lattice constant of the microtubule. These mechanical steps of kinesin are fast and completed within 15 $\mu$s.[10]

Kinesin exhibits tight coupling, i.e., it hydrolyzes one ATP molecule per mechanical step.[11] After ATP has been hydrolyzed by one of the catalytic motor domains, the inorganic phosphate is released rather fast, and both transitions together take of the order of 10 ms to be completed.[12] ADP is subsequently released from the catalytic domain, and this release process is also completed during about 10 ms.[13] Thus, these chemical transitions take much longer than the mechanical steps. When the catalytic domain of one motor head is occupied by ADP, this head is only loosely bound to the microtubule[14–16] and most likely to unbind from it.

We have recently developed a general theoretical framework for this chemomechanical coupling which shows that the single-step regime is governed by *several competing motor cycles*.[17,18] For kinesin, we have identified three cycles that dominate the single-step dynamics depending on the ATP, ADP, and P concentrations as well as on the load force.[19,20] The corresponding network of motor cycles provides a unified description for all motor properties that have been determined by single molecule experiments. For kinesin, the experimentally observed properties include

motor velocity,[10,21,22] bound state diffusion coefficient (or randomness parameter),[21] ratio of forward to backward steps,[10] dwell time distributions,[10] and run length[23] as functions of ATP concentration and load force as well as motor velocity as a function of P and ADP concentration.[24]

The directed stepping regime corresponds to the directed walks of the motor along the filament. Because of thermal noise, the motor makes, on average, a certain number of steps before it detaches from the filament. A single kinesin motor, for example, unbinds from the filament after the motor has made about a hundred steps, i.e., after a run length (or walking distance) of about $1\,\mu$m.[25] On length scales that are large compared to its run length, a single motor undergoes composite walks consisting of directed (or biased) motion along the filaments interrupted by diffusive (or random) motion in the surrounding solution.[26–29]

The run length of single motors is rather small compared to the long distances — centimeters or even meters — over which cargo particles such as vesicles or organelles are transported in cells and axons, see Fig. 2. One rather effective way to increase the run length is via cooperative transport of cargo particles by several motor molecules.[30] The corresponding run length distribution has been recently measured for two different in vitro assays.[31,32]

In eukaryotic cells, vesicles and other cargo particles, which are transported along microtubules, often carry both kinesins and dyneins which leads to bi-directional transport along the filaments.[33–35] The experimental observations for this type of transport are rather complex. The cargo may exhibit rather different types of trajectories with and without pauses between forward and backward motion. In addition, changing the molecular structure of one motor species often affects the movement in both directions. Therefore, it was proposed that this behavior reflects the coordination by an unknown protein complex attached to the cargo. However, we have recently shown that all experimental observations can be

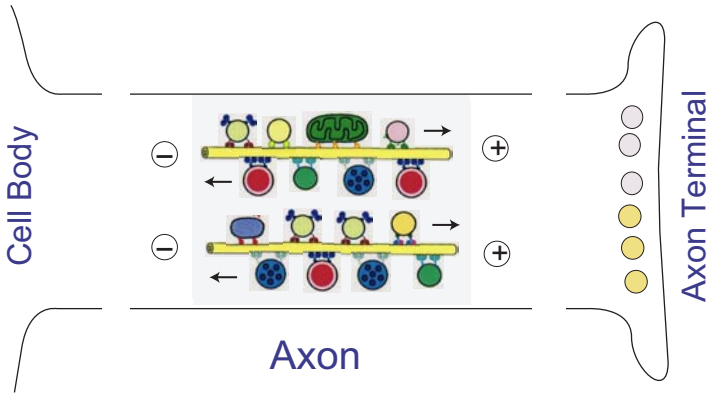


Fig. 2. Two-way traffic in an axon. The traffic is based on microtubules, which provide the tracks, and different types of cytoskeletal motors, which move along these filaments. Each motor species moves either towards the axon terminal (plus direction) or towards the cell body (minus direction). Small teams of motors pull vesicles and other types of cargo over macroscopic distances.

explained by a *stochastic tug-of-war* between the two motor species.[35] This implies that the signalling pathways that control intracellular transport may directly target the different motor molecules rather than an additional coordination complex.[35,36]

The cartoon in Fig. 2 indicates that the traffic within an axon can be rather dense and, thus, may lead to traffic jams as one would expect theoretically.[27,37–39] There is indeed some experimental evidence for jams of motor particles in axons (W. Saxton, private communication). An extreme case has been induced by mutations of the motor proteins which led to strong swelling of axons.[40,41] Jams of kinesin-like motors have also been observed in fungal hyphae as one varied the motor concentration in vivo by changing the level of expression of the corresponding gene.[42,43] Recently, motor traffic jams have also been observed in several in vitro experiments.[44–47] Apart from crowding and traffic jams, the mutual interaction between motors and filaments leads to *nonequilibrium phase transitions* as has been shown theoretically both for stepping motors on immobilized filaments[37,38,48] and for gliding filaments on immobilized motors.[49,50]

This review is organized as follows. The movements of single motors up to their run length are discussed in Sec. 2. The composite walks of single motors on larger length scales, are considered in Sec. 3. The effective diffusion coefficient of these walks can be enhanced by several orders of magnitude if the motors are in contact with certain filament patterns. Sec. 4 describes the cooperative transport of nanometer- or micrometer-sized cargo particles by several molecular motors. If all motors belong to the same molecular species, the cooperative action of the motors leads to uni-directional transport with a strongly increased run length, to the generation of larger forces, and to a characteristic force dependence of the velocity distributions, see Sec. 4.1. If two species of motors pull on the cargo in opposite directions, they perform a stochastic tug-of-war as described in Sec. 4.2. This tug-of-war leads to seven distinct motility regimes, two of which exhibit fast bi-directional transport. As mentioned, the complex experimental observations on bi-directional transport are all consistent with such a tug-of-war. Finally, the traffic of interacting motors and cargo particles is briefly discussed in Sec. 5. Depending on their interactions and the compartment geometry, the motors form various spatio-temporal patterns such as traffic jams and undergo nonequilibrium phase transitions between different patterns of transport.

## 2. Directed Stepping of Single Motors

In this section, the stepping regime of single motors up to their run length will be considered. First, we address the chemomechanical coupling between ATP hydrolysis and mechanical steps and describe a systematic theoretical framework for this coupling. This framework incorporates the catalytic ATPase activity of the motor domains as well as basic thermodynamic constraints. When applied to kinesin, it leads to a unified description of all single molecule data that have been obtained on

this motor. In addition, this framework also reveals that kinesin and other cytoskeletal motors are governed by several competing motor cycles.

### 2.1. *Thermodynamics of single motors*

Let us consider a single motor molecule bound to a filament that is embedded in a large amount of water at constant temperature $T$. During ATP hydrolysis, the motor binds ATP from the aqueous solution and releases ADP and P to it. In addition, the motor may experience a load force $F$ arising, e.g., from an optical trap. From the thermodynamic point of view, such a motor can be treated as a small system that is coupled to several reservoirs: (i) A heat reservoir at temperature $T$; (ii) A work reservoir characterized by the load force $F$; and (iii) Particle reservoirs for the chemical species $X = \text{ATP, ADP, and inorganic phosphate P}$. These different types of reservoirs are displayed in Fig. 3.

The motor is taken to be in thermal equilibrium with its environment, i.e., the motor is characterized by the same temperature $T$ as the surrounding solution. The heat exchanged between the motor and the reservoir will be denoted by $Q$. We use the sign convention that the exchanged heat $Q$ is positive if it increases the internal energy of the reservoir. Thus, $Q > 0$ corresponds to heat release from the motor to the reservoir.

Interaction of the molecular motor with the work reservoir is governed by the load force $F$. This force acts parallel to the filament and is taken to have a constant value independent of the spatial position of the motor. We use the sign convention that $F$ is positive if it acts against the prefered movement of the motor.[a] If the motor moves by the distance $\ell$ in its prefered direction along the filament, it performs the mechanical work

$$W_{\rm me} = \ell F > 0 \quad \text{for } F > 0. \tag{2.1}$$

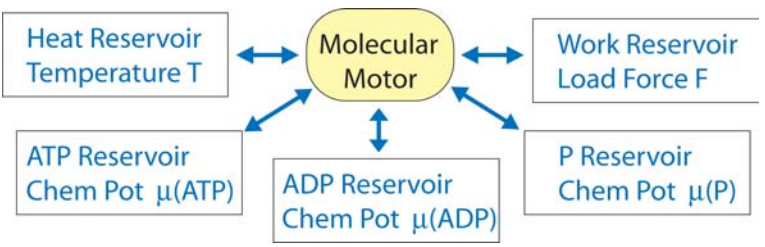


Fig. 3. Thermodynamic view of a molecular motor that is coupled to several reservoirs: a heat reservoir at temperature $T$; particle exchange reservoirs for ATP, ADP, and P with chemical potentials $\mu$(ATP), $\mu$(ADP), and $\mu$(P); and a work reservoir governed by load force $F$. The motor is always taken to be in thermal equilibrium at temperature $T$ but can be in chemical equilibrium or nonequilibrium depending on the size of the three chemical potentials. Mechanical equilibrium corresponds to $F = 0$.[18]

[a]This sign convention must be modified if one considers the action of both plus and minus directed motors, see Sec. 4.2.3 below.

Mechanical equilibrium between motor and work reservoir corresponds to $F = 0$.

In general, the external force as applied in single molecule experiments is a 3-dimensional vector with one component parallel to the filament defining the load force and additional components acting perpendicular to this filament. Since the motor does not perform mechanical work against the perpendicular force components, the latter components do *not* represent thermodynamic control parameters, even though they can affect the motor dynamics.[18]

The exchange equilibria between the motor and the reservoirs for the chemical species $X$ = ATP, ADP, and P are governed by the corresponding chemical potentials, $\mu(X)$. The activity of $X$ will be denoted by $[X]$ and is equal to the molar concentration in the limit of dilute solutions. In the following, we will use the term 'concentration' to be a synonym for 'activity'. For each activity $[X]$, we choose the activity scale $[X]^*$ in such a way that the chemical potential $\mu(X)$ has the simple form

$$\mu(X) = k_B T \ln([X]/[X]^*) \tag{2.2}$$

with the Boltzmann constant $k_B$.[b]

When the motor hydrolyzes a single ATP molecule, it binds one such molecule and releases one inorganic phosphate P and one ADP molecule. According to the Gibbs fundamental form of thermodynamics, the corresponding change in internal energy of the motor is given by the chemical energy difference

$$\Delta\mu = \mu(\mathrm{ATP}) - \mu(\mathrm{P}) - \mu(\mathrm{ADP}) \tag{2.3}$$

which also represents the chemical energy input from the aqueous solution to the motor molecule. Using the expression (2.2) for the three chemical potentials, we then obtain

$$\Delta\mu = k_B T \ln\left(\frac{[\mathrm{ATP}]}{[\mathrm{ADP}][\mathrm{P}]} K^{\mathrm{eq}}\right) \quad \text{with } K^{\mathrm{eq}} \equiv \frac{[\mathrm{ADP}]^*[\mathrm{P}]^*}{[\mathrm{ATP}]^*} \tag{2.4}$$

which defines the equilibrium (dissociation) constant $K^{\mathrm{eq}}$. Chemical equilibrium between ATP hydrolysis and ATP synthesis corresponds to $\Delta\mu = 0$ which implies

$$K^{\mathrm{eq}} = \left.\frac{[\mathrm{ADP}][\mathrm{P}]}{[\mathrm{ATP}]}\right|^{\mathrm{eq}} . \tag{2.5}$$

For dilute solutions, the activities of the three chemical species are equal to their molar concentrations and can be directly measured, at least in principle (after the system has relaxed into chemical equilibrium). For ATP hydrolysis, the precise value of the equilibrium constant $K^{\mathrm{eq}}$ depends on the ionic conditions but a typical value

[b]In general, the activity $[X]$ is defined in such a way that the chemical potential $\mu_X$ for the chemical species $X$ has the simple form $\mu_X \equiv \mu_X^o + k_B T \ln([X]/[X]^o)$ where the superscript $o$ refers to some standard or reference activity $[X]^o$. This relation can be rewritten in the form $[X]^o e^{-\mu_X^o/k_B T} = [X] e^{-\mu_X/k_B T}$ which holds for *any* reference state. Therefore, the right hand side of this equation can be used to define the activity scale $[X]^* \equiv [X] e^{-\mu_X/k_B T}$ which has a unique value independent of the reference activity $[X]^o$.

is given by $K^{\rm eq} = 4.9 \times 10^{11}\ \mu$M.[24,51] Thus, in thermal equilibrium at temperature $T$, a single molecular motor is governed by four thermodynamic control parameters, namely the three activities or concentrations $[X]$ with $X =$ ATP, ADP, and P as well as the load force $F$ or, equivalently, the three chemical potentials $\mu(X)$ and $F$.

Since the chemical energy input $\Delta\mu$ as given by (2.4) depends on all three concentrations [ATP], [ADP], and [P], the limit, in which one of these concentrations becomes small, is not defined unless one specifies the two remaining concentrations as well. If one considers the limit of small [ATP] for fixed [ADP] and [P], for example, the chemical energy input $\Delta\mu$ goes to minus infinity. Likewise, if one considers the limit of small [ADP] and/or small [P] for fixed [ATP], the energy input $\Delta\mu$ goes to plus infinity. Furthermore, if all three concentrations become small with $[\text{ATP}] \approx [\text{ADP}][\text{P}]/K$ with a certain, fixed activity or concentration $K$, $\Delta\mu$ attains the limiting value $\Delta\mu = \ln(K^{\rm eq}/K)$. Thus, even if all three concentrations vanish simultaneously, the limiting value of $\Delta\mu$ depends on how they vanish.

In the absence of ATP, ADP, and P, the motor does not obtain any chemical energy and, thus, cannot perform any mechanical work. Thus, one would like to view this situation as a limiting case of chemical equilibrium with $\Delta\mu = 0$. The latter value is obtained if all three concentrations vanish simultaneously with the constraint that $[\text{ATP}] \approx [\text{ADP}][\text{P}]/K^{\rm eq}$.

### 2.2. *Enzymatic activity of motor molecules*

For a given position at the filament, the molecular motor can attain many molecular conformations, which differ in the chemical composition of their catalytic domains and in thermally excited vibrational modes. Since we want to describe the hydrolysis of single ATP molecules, we will use a *discrete* state space and focus on the different chemical compositions of the catalytic domains. From a mathematical point of view, the chemical composition of the catalytic domains provides an equivalence relation that divides the molecular configurations of the motor into mutually distinct sets or equivalence classes.

We start with a single catalytic domain as shown in Fig. 4(a) and (b). Such a catalytic domain can be occupied by a single ATP molecule, by the combination ADP/P, by a single ADP molecule, or can be empty. In this way, each catalytic domain can attain 4 different states, as shown in Fig. 4(a) where these states are represented as vertices in a network graph. Such a representation was previously used by T. L. Hill[52] for a generic ATPase. The edges between the different chemical states in Fig. 4(a) represent forward and backward transitions. The edge between state $i$ and state $j$ will be denoted by $\langle ij \rangle$. It consists of two directed edges or di-edges, $|ij\rangle$ and $|ji\rangle$, corresponding to the forward transition from $i$ to $j$ and to the backward transition from $j$ to $i$, respectively. Thus, the di-edge or transition $|\text{ET}\rangle$ corresponds to ATP binding to the catalytic domain whereas the transition $|\text{TE}\rangle$ represents ATP release from this domain. Likewise, the transitions $|\Theta\text{D}\rangle$, $|\text{D}\Theta\rangle$, $|\text{DE}\rangle$, and $|\text{ED}\rangle$ describe P release, P binding, ADP release, and ADP binding,

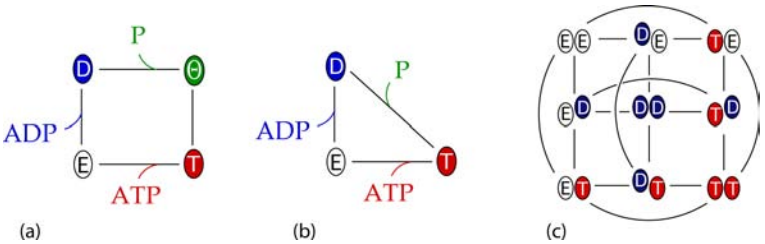


Fig. 4. Chemical networks (a, b) for a single catalytic motor domain acting as an ATPase, and (c) for a motor with two catalytic motor domains. In (a), the catalytic motor domain can be empty (E), occupied by ATP (T), by ADP/P (Θ), or by ADP (D). In (b), the cleavage transition $|T\Theta\rangle$ and the P release transition $|\Theta D\rangle$ have been combined into the single transition $|TD\rangle$ leading to a reduced network with the three states E, T, and D. In (c), the same three states are accessible to each motor domain which implies a chemical network with $3^2 = 9$ states. Each solid line between two vertices $i$ and $j$ corresponds to both the forward chemical transition $|ij\rangle$ and the backward chemical transition $|ji\rangle$. Thus, the 9-state network in (c) contains 18 forward and 18 backward transitions.

respectively. Finally, the transition $|\mathrm{T}\Theta\rangle$, corresponds to ATP cleavage and the transition $|\Theta\mathrm{T}\rangle$ to ATP synthesis from the ADP/P state.

The three edges $\langle\mathrm{ET}\rangle$, $\langle\Theta\mathrm{D}\rangle$, and $\langle\mathrm{DE}\rangle$ involve the binding and release of a certain molecular species from the aqueous solution. In contrast, the edge $\langle\mathrm{T}\Theta\rangle$ in the 4-state network does not involve such an interaction of the catalytic domain with the particle reservoir, see Fig. 4(a). Therefore, one may combine the two edges $\langle\mathrm{T}\Theta\rangle$ and $\langle\Theta\mathrm{D}\rangle$ of the 4-state network into the edge $\langle\mathrm{TD}\rangle$ as shown in Fig. 4(b). The latter representation involves only 3 states: the motor head is occupied by ADP in state D, empty in state E, and occupied by ATP in state T. This reduced representation can be defined in such a way that the 3-state and the 4-state network describe the same energy transduction process as shown in Ref. 18.

Next, we consider a two-headed motor such as kinesin or myosin V with two identical catalytic motor domains. If each motor domain can attain three different chemical states as in Fig. 4(b), the two-headed motor can attain $3^2 = 9$ different states as in Fig. 4(c).[19]

It is straightforward to generalize these considerations to a molecular motor with $M$ catalytic domains. In this case, the different chemical compositions of the motor domains define $3^M$ motor states, which are represented by $3^M$ vertices. Each of these vertices is connected to $2M$ other vertices via chemical transitions, i.e., each vertex has 'chemical degree' $2M$. As a result, one obtains a network with $M3^M$ chemical edges, each of which represents both a forward and a backward chemical transition. This network represents an $M$-dimensional hypercube with periodic boundary conditions.

### 2.3. *Chemomechanical coupling*

Next, we must complement the chemical network as shown in Fig. 4(c) by mechanical transitions that represent the spatial displacements of the motors along the

filaments. We will now use the convention that, for each state in Fig. 4(c), the right head is the leading head whereas the left head is the trailing head with respect to the prefered direction of the motor movement.

### 2.3.1. *Network representations*

Both the kinesin motor[8,9] and the myosin V motor[53] walk in a hand-over-hand fashion, i.e., by alternating steps, in which one head moves forward while the other one remains bound to the filament. In addition, recent experiments[10] provide strong evidence for the kinesin motor that the time scales for the mechanical and chemical transitions are well separated: the mechanical transitions are completed within a few microseconds whereas the chemical transitions take many milliseconds. If we incorporate these two properties into the network representation, we obtain nine possible mechanical transitions as shown in Fig. 5. For myosin V, the motor undergoes two[54] or three[55] mechanical substeps which implies that some of the chemical states are located at intermediate positions between the binding sites of the filament.

In principle, one may now construct a variety of chemomechanical networks by including different subsets of the possible mechanical transitions shown in Fig. 5(a)–5(c). In general, this would lead to many possible pathways, a viewpoint that has been previously emphasized for somewhat different network representations[56,57] that did not include the chemical species ADP and P. In practise, the chemomechanical networks obtained from Fig. 5(a)–5(c) can be simplified substantially as has been explicitly shown for kinesin in Ref. 19.

For kinesin, the T and the E state of each motor head are strongly bound whereas the D state is only weakly bound to the filament.[14–16] In order to make a forward mechanical step, the trailing head must detach from the filament whereas the leading head must be firmly attached to it. It is then implausible that the motor starts its mechanical step from any state in which the trailing head is strongly bound and/or the leading head is weakly bound to the filament. This implies that the motor is unlikely to undergo this transition from the (ED), (TD) or (DD) states as well as from the (ET), (TE), (EE), or (TT) states. One is then left with only two possible mechanical transitions in the forward direction, from state (DE) to state (ED) and from state (DT) to (TD).

If the motor underwent its mechanical transition starting from the (DE) state, this mechanical transition would compete with the transition from (DE) to (DT). Since the transition rate for the latter transition increases with the ATP concentration, the frequency for the (DE) to (DT) transition would increase and the frequency for the (DE) to (ED) transition would decrease with increasing ATP concentration. Therefore, if the motor underwent its mechanical transition from (DE) to (ED), its velocity would decrease for high ATP concentration. Since such a decrease of motor velocity with ATP concentration is not observed experimentally, one concludes that

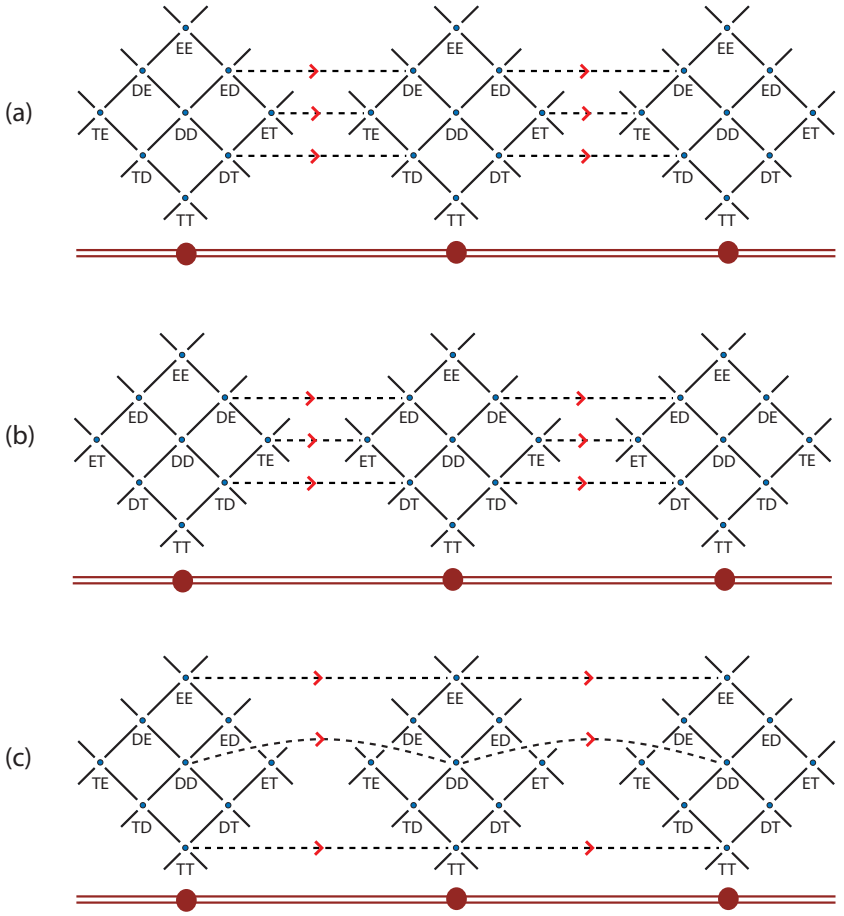


Fig. 5. Possible mechanical transitions or steps between the chemical motor states at different binding sites of the filament. In principle, one has nine such transitions starting from the nine chemical motor states. For the sake of clarity, these nine possibilities have been divided up into three subgroups in subfigures (a), (b), and (c). The thick double-lines at the bottom of each subfigure represent the filament, the three bullets on these lines three filament binding sites. The motor can attain nine chemical states at each binding site. The solid and broken lines of the networks correspond to chemical and mechanical transitions, respectively. The arrows (red) indicate the forward direction of the mechanical transitions. The chemical networks have been drawn as square lattices with periodic boundary conditions; the stubs correspond to additional chemical transitions that connect the boundary states of these square lattices.

the mechanical forward transition of kinesin corresponds to the transition from the (DT) to the (TD) state.[c] Thus, kinesin should be governed by the chemomechanical network in Fig. 6 as proposed in Ref. 19.

[c]In principle, the motor could also undergo the (DT) to (TD) transition with high frequency and (DE) to (ED) transition with low freqency but, at present, there is no experimental evidence for such a more complex stepping process.

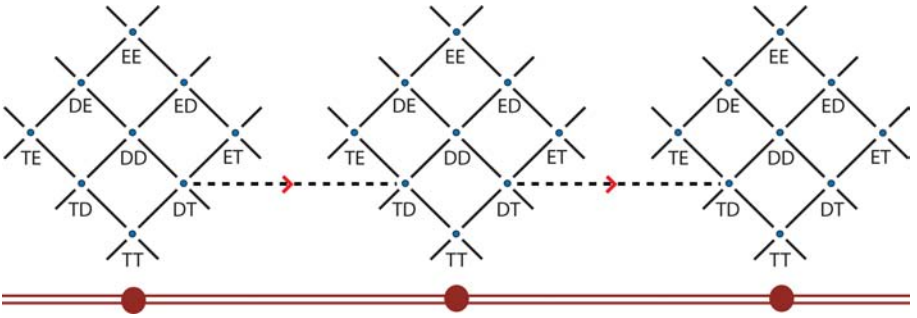


Fig. 6. Mechanical forward transition from state (DT) to state (TD) that should dominate for kinesin.

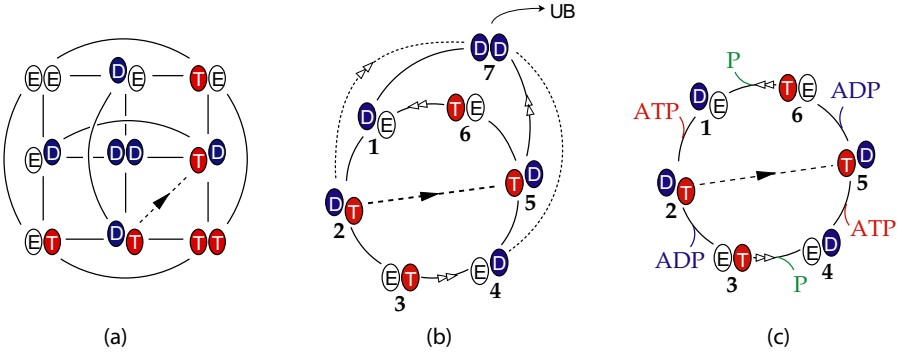


Fig. 7. Chemomechanical networks for the processive motion of kinesin with chemical (solid lines) and mechanical (broken lines) transitions: (a) Compact representation of the periodic network in Fig. 6; (b) Reduced 7-state network without the most strongly bound motor states (TT) and (EE); and (c) Reduced 6-state network without the most weakly bound motor state (DD). The white double-arrows indicate the direction of ATP hydrolysis, the black arrows the direction of mechanical forward steps.[19]

A more compact and equivalent representation for the kinesin network in Fig. 6 is shown in Fig. 7(a). Indeed, to each trajectory in the periodic network of Fig. 6, there is a corresponding trajectory in the compact network of Fig. 7(a) and vice versa. In addition, the spatial displacement along the filament can be recovered from the trajectories in the compact network of Fig. 7(a) by simply counting the number of forward and backward mechanical transitions from (DT) to (TD) and from (TD) to (DT), respectively.

The chemomechanical network as shown in Fig. 7(a) contains 36 chemical forward and backward transitions in addition to the forward and backward mechanical transitions. On the one hand, it is not possible at present to uniquely determine all of these rates from the available experimental data. On the other hand, it turns out that all of these data can be quantitatively described by the reduced 7-state network in Fig. 7(b) in which the two most strongly bound states (TT) and (EE)

have been omitted. Indeed, it is a priori unlikely that the motor visits these two states during its processive motion. An even simpler description is obtained if one ignores the (DD) state as well which leads to the 6-state network in Fig. 7(c). The latter network is sufficient to describe all single motor data currently available apart from the strong reduction of the motor velocity with increasing ADP concentration.[19]

### 2.3.2. *Cycles and dicycles*

The previous subsections provided some examples for the description of molecular motors in terms of a discrete state space. These states are represented as the vertices of a network graph, $\mathbb{G}$, and are labeled by $i = 1, 2, \ldots, |\mathbb{G}|$. Two neighboring states $i$ and $j$ are connected by an edge $\langle ij \rangle$ which represents the two directed edges or transitions $|ij\rangle$ and $|ji\rangle$. Inspection of Fig. 7(a)–7(c) shows that these edges form cycles. These cycles are particularly important in the present context since they are intimately related to fluxes and nonequilibrium steady states.

In order to be precise, we will distinguish (undirected) cycles from directed cycles or *dicycles*. The smallest dicycle consists of three states and three di-edges. An (undirected) cycle $\mathcal{C}_\nu$ is given by a closed sequence of neighboring vertices together with connecting edges, in which each vertex and each edge occurs only once. Each cycle $\mathcal{C}_\nu$ leads to two dicycles $\mathcal{C}_\nu^d$ with $d = \pm$.

The network description of a single motor head, see Fig. 4 (a,b), involves only a single cycle. Analogous unicycle models have also been frequently used for two-headed motors. Inspection of Fig. 7 shows, however, that these two-headed motors will, in general, exhibit several motor cycles. The 9-state network in Fig. 7(a) involves a rather large number of cycles (more than 200). In contrast, the 6-state network in Fig. 7(c) contains only three cycles: the forward cycle $\mathcal{F} = \langle 25612 \rangle$, the backward cycle $\mathcal{B} = \langle 52345 \rangle$, and the dissipative slip cycle $\mathcal{D} = \langle 1234561 \rangle$.

### 2.3.3. *Energy balance conditions*

Each dicycle $\mathcal{C}_\nu^d$ can be characterized by several energies: the chemical energy $\Delta\mu(\mathcal{C}_\nu^d)$ that the motor gains during the completion of $\mathcal{C}_\nu^d$, the mechanical work $W_{\rm me}(\mathcal{C}_\nu^d)$ that it performs during this completion, and the heat $Q(\mathcal{C}_\nu^d)$ that it releases to its environment or heat reservoir. These different energies satisfy the energy balance relation

$$\Delta\mu(\mathcal{C}_\nu^d) - W_{\rm me}(\mathcal{C}_\nu^d) = Q(\mathcal{C}_\nu^d) \tag{2.6}$$

as follows from the first law of thermodynamics.

In order to obtain a quantitative model for the motor dynamics, one has to specify the transition rates $\omega_{ij}$ for transitions $|ij\rangle$ between the motor states $i$ and

$j$. As shown in Refs. 17 and 18, the released heat $Q(\mathcal{C}_\nu^d)$ is related to the transition rates $\omega_{ij}$ by

$$Q(\mathcal{C}_\nu^d) \equiv k_B T \bar{Q}(\mathcal{C}_\nu^d) = k_B T \ln\left(\frac{\Pi_\omega(\mathcal{C}_\nu^d)}{\Pi_\omega(\mathcal{C}_\nu^{-d})}\right) \tag{2.7}$$

with the transition rate products

$$\Pi_\omega(\mathcal{C}_\nu^d) \equiv \prod_{|ij\rangle}^{\nu,d} \omega_{ij}, \tag{2.8}$$

where the product includes all directed edges or transitions of the dicycle $\mathcal{C}_\nu^d$. The energy balance relation (2.7) is consistent with the proposal in Ref. 58 that the entropy produced during a single transition is equal to $k_B T \ln(\omega_{ij}/\omega_{ji})$. This relation can also be rewritten in a form that is reminiscent of the various fluctuation theorems for entropy fluctuations[59–62] as explained in Ref. 18.

A combination of the relations (2.6) and (2.7) then leads to the dicycle balance conditions[17,18]

$$k_B T \ln\left(\frac{\Pi_\omega(\mathcal{C}_\nu^d)}{\Pi_\omega(\mathcal{C}_\nu^{-d})}\right) = \Delta\mu(\mathcal{C}_\nu^d) - W_{\rm me}(\mathcal{C}_\nu^d) \tag{2.9}$$

for the transition rates $\omega_{ij}$. Indeed, the chemical energy $\Delta\mu(\mathcal{C}_\nu^d)$ can be expressed in terms of the chemical energy difference $\Delta\mu$ obtained from the hydrolysis of a single ATP molecule as given by (2.3), and the mechanical work $W_{\rm me}(\mathcal{C}_\nu^d)$ depends on the load force $F$ and on the step size $\ell$, compare (2.1). Therefore, the balance conditions (2.9) represent thermodynamic constraints on the kinetics. Note that the balance conditions for $\mathcal{C}_\nu^+$ and $\mathcal{C}_\nu^-$ differ only by an overall sign and are, thus, linearly dependent. In fact, the number of linearly independent balance conditions is equal to the number of fundamental cycles of the network.

### 2.3.4. *Motor dynamics for processive stepping*

For the 6-state network of kinesin as displayed in Fig. 7(c), one has three cycles and two fundamental ones; for the 7-state network in Fig. 7(b) without the two dotted edges, one has six cycles and three fundamental ones. When these networks are supplemented by the associated balance conditions, one obtains a rather good description for all properties of the kinesin motor as experimentally observed in single motor experiments.[19] In these experiments, the average motor velocity $v$ has been measured as a function of the ATP, ADP, and P concentrations as well as of the load force $F$. The latter dependence is shown in Fig. 8(a) with the experimental data of Carter and Cross[10] and the result of the network calculations as obtained in Ref. 19. Inspection of Fig. 8(a) shows very good agreement between theory and experiment. Likewise, the network calculations provide a very good description for the data reported in Refs. 21–24.

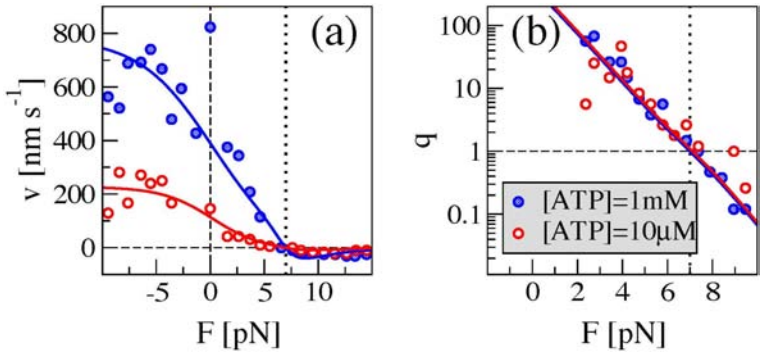


Fig. 8. (a) Average motor velocity $v$ and (b) forward to backward step ratio $q$ for the kinesin motor as a function of load force $F$ for two different values of the ATP concentration. The experimental data are from Ref. 10. The solid lines are from Ref. 19 and have been calculated using the chemomechanical networks in Figs. 7(b) and 7(c). At the stall force $F = F_{\rm s} \simeq 7$ pN indicated by the vertical dotted line, the velocity $v$ vanishes and the step ratio $q = 1$.

Another important consequence of the balance conditions (2.9) is that they determine the general form of the dicycle excess fluxes in the steady state. The latter fluxes are defined via[17,18]

$$\Delta J^{\rm st}(\mathcal{C}_\nu^d) \equiv J^{\rm st}(\mathcal{C}_\nu^d) - J^{\rm st}(\mathcal{C}_\nu^{-d}), \tag{2.10}$$

i.e., by the difference of the steady state dicycle fluxes $J^{\rm st}(\mathcal{C}_\nu^d)$ with $d = \pm$. The dicycle fluxes have the general properties

$$J^{\rm st}(\mathcal{C}_\nu^d) > 0 \quad \text{and} \quad J^{\rm st}(\mathcal{C}_\nu^d) \propto \Pi_\omega(\mathcal{C}_\nu^d) \tag{2.11}$$

with a proportionality factor that depends only on the cycle $\mathcal{C}_\nu$ but not on its direction $d = \pm$ as can be explicitly shown using the graph-theoretic or diagrammatic solution for the steady state probabilities (often refered to as the Kirchhoff method). Using the relation between the transition rate products $\Pi_\omega$ and the released heat $Q(\mathcal{C}_\nu^d)$ as given by (2.7), one concludes that the dicycle excess fluxes have the generic form

$$\Delta J^{\rm st}(\mathcal{C}_\nu^d) = [1 - e^{-\bar{Q}(\mathcal{C}_\nu^d)}] J^{\rm st}(\mathcal{C}_\nu^d). \tag{2.12}$$

Since the flux $J^{\rm st}(\mathcal{C}_\nu^d)$ is always positive, the expression (2.12) for the dicycle excess flux implies that

$$\text{sign of } \Delta J^{\rm st}(\mathcal{C}_\nu^d) = \text{sign of } \bar{Q}(\mathcal{C}_\nu^d) \tag{2.13}$$

and that

$$\Delta J^{\rm st}(\mathcal{C}_\nu^d) = 0 \quad \text{if and only if } \bar{Q}(\mathcal{C}_\nu^d) = 0, \tag{2.14}$$

i.e., the dicycle excess flux $\Delta J^{\rm st}(\mathcal{C}_\nu^d)$ vanishes for those values of the thermodynamic control parameters for which the released heat $\bar{Q}(\mathcal{C}_\nu^d)$ vanishes.

Since the released heat $\bar{Q}$ is a thermodynamic quantity, thermodynamics alone determines the sign and the zeros of all dicycle excess fluxes $\Delta J^{\rm st}(\mathcal{C}_\nu^d)$ in the steady

state. Many experimentally accessible quantities such as the motor velocity and the ATP hydrolysis rate correspond to linear combinations of the dicycle excess fluxes. Using the above mentioned properties of the dicycle excess fluxes both for the motor velocity and the ATP hydrolysis rate, one can identify four different operation modes for kinesin.[63]

### 2.3.5. *Motor velocity and stall force*

The force-velocity relationship as shown in Fig. 8(a) for kinesin represents an important property of all stepping motors. In Fig. 8(a), we used the convention that the force $F$ is positive if it decreases the probability that the motor makes forward steps. As long as we consider single motors, this convention will be used for any motor species irrespective of its preferential stepping direction. If the force acts simultaneously on plus directed and minus directed motors, we need to modify this convention, see Sec. 4.2 below. Inspection of Fig. 8(a) shows that the motor velocity decreases with increasing load force $F$ and vanishes at a characteristic force scale, the stall force $F = F_{\rm s}$. Intuitively, one may view this stall force as the maximal force that can be generated by the motor.

For the kinesin networks in Figs. 7(b) and 7(c), the parameter dependence of this stall force can be determined explicitly. In these networks, the motor velocity is proportional to the excess flux $\Delta J^{\rm st}_{25} = P^{\rm st}_2 \omega_{25} - P^{\rm st}_5 \omega_{52}$ from state 2 to state 5 with the steady state probabilities $P^{\rm st}_2$ and $P^{\rm st}_5$ to find the motor in state 2 and 5, respectively. For the 6-state network in Fig. 7(c), one then has[19]

$$v = \ell \Delta J^{\rm st}_{25} = \ell[\Delta J^{\rm st}(\mathcal{F}^+) - \Delta J^{\rm st}(\mathcal{B}^+)] \tag{2.15}$$

with the step size $\ell$ and the two dicycles $\mathcal{F}^+ = |25612\rangle$ and $\mathcal{B}^+ = |23452\rangle$. For the transition rates as chosen in Ref. 19, the motor velocity vanishes at the rescaled stall force

$$\bar{F}_{\rm s} \equiv \frac{\ell F_{\rm s}}{k_B T} = \ln\left(\frac{e^{\bar{F}_\infty} + e^{-\Delta\bar{\mu}}}{1 + e^{\bar{F}_\infty - \Delta\bar{\mu}}}\right) \tag{2.16}$$

with $\Delta\bar{\mu} \equiv \Delta\mu/k_B T$ and $\bar{F}_\infty \equiv \ln[\omega_{25}(F=0)/\omega_{52}(F=0)]$. The relation (2.16) leads to the asymptotic behavior

$$\bar{F}_{\rm s} \approx \bar{F}_\infty \quad \text{for large} \quad \Delta\bar{\mu} \tag{2.17}$$

and

$$\bar{F}_{\rm s} \approx \frac{e^{\bar{F}_\infty} - 1}{e^{\bar{F}_\infty} + 1} \Delta\bar{\mu} \quad \text{for small} \quad \Delta\bar{\mu}. \tag{2.18}$$

Since $k_B T/\ell = 0.5\,\text{pN}$ at room temperature, the value $F_\infty \simeq 7\,\text{pN}$ as determined experimentally[10,21] implies $\bar{F}_\infty \simeq 14$. An explicit expression for the stall force can also be obtained for the 7-state network in Fig. 7(b). In fact, analyzing both the motor velocity and the ATP hydrolysis rate, one can identify four different operation modes for kinesin as described in Ref. 63.

### 2.3.6. *Dwell time distributions for mechanical steps*

In single motor experiments using optical traps, one can observe the spatial position of the motor as a function of time. For low ATP concentrations, the motor dwells in a certain position along the filament and, then, makes a fast mechanical transition to a new spatial position. If one measures many dwell times between successive mechanical transitions, one obtains the dwell time distributions of the motor.

As pointed out in Ref. 20, there are, in fact, four different dwell time distributions corresponding to the four possible pairs of subsequent forward and backward steps, namely forward-after-forward steps, forward-after-backward steps, backward-after-forward steps, and backward-after-backward steps. For kinesin, these dwell time distributions have been calculated starting from the 6-state network in Fig. 7(c).[20] Two of these four distributions are displayed in Fig. 9. Inspection of this figure shows that these distributions have a strongly non-exponential character reflecting the underlying network dynamics involving chemical transitions between the different motor states.

The dwell time distributions for kinesin can be calculated from the extended network in Fig. 10 which is obtained from the 6-state network in Fig. 7(c) by the addition of the two absorbing states $j = 2'$ and $j = 5'$. On this extended network, the motor starts in the initial state $i = 5$ after a forward step or in the initial state $i = 2$ after a backward step. One then considers the probability $P_{ij}(t)$ that the motor is 'absorbed' after time $t$ in state $j = 5'$ corresponding to a final forward step or in state $j = 2'$ corresponding to a final backward step.

The corresponding absorption times $t^{\rm ab}_{i|j}$ are governed by the probabilities[20]

$$\Pr\{t^{\rm ab}_{i|j} \le t\} = \int_0^t du \rho^{\rm ab}_{i|j}(u) \tag{2.19}$$

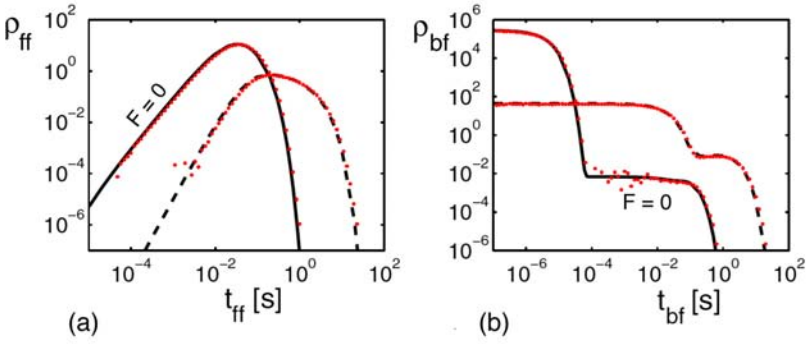


Fig. 9. (a) Probability distribution $\rho_{\rm ff}$ for the dwell time $t_{\rm ff}$ of mechanical forward-after-forward steps, i.e., the dwell time between two successive forward steps; and (b) Probability distribution $\rho_{\rm bf}$ for the dwell time $t_{\rm bf}$ of mechanical forward-after-backward steps. In both cases, one curve corresponds to vanishing load force $F = 0$ (as indicated), the other to $F = F_{\rm s}$, i.e., the load force being equal to the stall force. In addition, the motor dynamics leads to the probability densities $\rho_{\rm fb}$ und $\rho_{\rm bb}$ for backward-after-forward steps and backward-after-backward steps, respectively.[20]

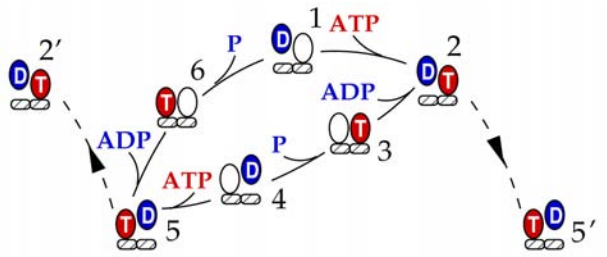


Fig. 10. Extended (6+2)-state network for kinesin as obtained from the 6-state network in Fig. 7(c) by adding the two adsorbing states $j = 2'$ and $j = 5'$. The motor undergoes a forward-after-forward step if it starts initially in state $i = 5$ and is subsequently 'absorbed' in state $j = 5'$. Likewise, the motor undergoes a forward-after-backward step if it starts initially in state $i = 2$ and is subsequently 'absorbed' in state $j = 5'$.

with the probability distribution[d]

$$\rho_{i|j}^{\rm ab}(t) = \frac{\partial}{\partial t} P_{ij}(t)/P_{ij}^{\rm st}, \tag{2.20}$$

where $P_{ij}^{\rm st}$ is the steady state solution for the probability $P_{ij}(t)$. Thus, the two probability distributions $\rho_{\rm ff}$ and $\rho_{\rm bf}$ as displayed in Fig. 9 are obtained from the relations[20]

$$\rho_{\rm ff}(t) = \frac{\partial}{\partial t} P_{55'}(t)/P_{55'}^{\rm st} \quad \text{and} \quad \rho_{\rm bf}(t) = \frac{\partial}{\partial t} P_{25'}(t)/P_{25'}^{\rm st}; \tag{2.21}$$

the two remaining dwell time distributions $\rho_{\rm fb}$ and $\rho_{\rm bb}$ for backward-after-forward steps and backward-after-backward steps can be calculated in an analogous fashion.

Linear combinations of the four dwell time distributions $\rho_{\rm ff}$, $\rho_{\rm bf}$, $\rho_{\rm fb}$, and $\rho_{\rm bb}$ determine the probability distributions for forward and backward steps.[20] For kinesin, the latter distributions have been determined experimentally.[10] More precisely, these distributions have been measured for dwell times that exceed a certain small time cutoff that varies between 0.01 and 0.1 s depending on ATP concentration and load force. As shown in Ref. 20, these experimental data are very well described by the theoretical distributions as calculated for the 6-state network of kinesin. This agreement is quite remarkable since all transition rates used in this calculation have been obtained in Ref. 19 without any reference to the dwell time distributions. Thus, the agreement between theory and experiment is obtained without any additional fitting parameter.

### 2.4. *Unbinding rate and run length*

The processive motors displayed in Fig. 1 can make many successive steps corresponding to many successive motor cycles. However, even if the motor's binding

[d]In mathematics, the quantity $\rho_{i|j}^{\rm ab}(t)$ is called a probability density function.

energy is large compared to the thermal energy $k_BT$, thermal fluctuations will eventually lead to an unbinding of the motor from the filament. Thus, a single motor can be characterized by its average run time $\langle \Delta t \rangle$ and the corresponding unbinding rate

$$\omega_{\rm off} \equiv 1/\langle \Delta t \rangle. \tag{2.22}$$

During its run time, the single motor steps along the filament and covers the average run length

$$\langle \Delta x \rangle = v \langle \Delta t \rangle. \tag{2.23}$$

In the absence of load, kinesin motors bound to microtubules make about 100 successive steps[25] which corresponds to an average run length $\langle \Delta x \rangle \simeq 1\,\mu$m and an average run time $\langle \Delta t \rangle \simeq 1$ s. In the absence and presence of dynactin, an accessory protein, dynein motors make about 20 and 40 successive steps, respectively.[64] Myosin V, which moves along actin filaments, makes about 50 steps before it unbinds again corresponding to a run length of about $1.5\,\mu$m.[65] Myosin VI, on the other hand, makes only about 9 successive steps, i.e., its average run length is about 280 nm.[66]

For a single motor stepping along a uniform filament as considered here, the motor's run time is equal to the motor's binding time, i.e., the time during which the motor is bound to the filament. In general, these two time scales can be different. Two examples are provided by a single motor that encounters defects on the filaments or by a cargo particle that is pulled by two antagonistic motor teams as discussed in Sec. 4.2 below. In these latter cases, the run times are shorter than the binding times.

The unbinding of a single motor is an activated process governed by a corresponding energy barrier. In the presence of an external force $F$ that acts to detach the motor, this barrier is reduced by $F\ell_{\rm d}$ where $\ell_{\rm d}$ represents an appropriate molecular length scale, which characterizes the elastic deformation of the motor molecule required for its detachment. Therefore, the unbinding rate $\omega_{\rm off}$ is expected to have the general form

$$\omega_{\rm off}(F) = \kappa_{\rm off} \exp(\ell_{\rm d} F/k_BT) \equiv \kappa_{\rm off} \exp(F/F_{\rm d}) \tag{2.24}$$

as follows from Kramers theory for activated processes with the zero-force unbinding rate $\kappa_{\rm off}$ and the detachment force

$$F_{\rm d} \equiv k_BT/\ell_{\rm d}. \tag{2.25}$$

Now, let us again focus on the network representations for kinesin as displayed in Fig. 7. In order to describe the unbinding of the motor from the filament, we must extend these networks by unbound motor states as indicated by 'UB' in Fig. 7(b).

It is convenient to label these unbound states by $i = 0$. Thus, if the motor dwells in a state $i > 0$, its unbinding rate $\omega_{i0}$ should have the load dependent form

$$\omega_{i0} = \kappa_{i0} \exp(\ell_{\mathrm{d},i} F/k_B T) \equiv \kappa_{i0} \exp(F/F_{\mathrm{d},i}) \equiv \kappa_{i0} \exp(\chi_{i0} \bar{F}) \tag{2.26}$$

which defines the zero-force unbinding rates $\kappa_{i0}$, the detachment forces $F_{\mathrm{d},i} \equiv k_B T/\ell_{\mathrm{d},i}$, the dimensionless parameters $\chi_{i0} \equiv \ell_{\mathrm{d},i}/\ell$, and the dimensionless force $\bar{F} \equiv \ell F/k_B T$, compare (2.16). Intuitively, one may view the detachment force $F_{\mathrm{d},i}$ as the maximal force that the motor can sustain in motor state $i$.

The most weakly bound state of kinesin is provided by the (DD)-state. Thus, in order to reduce the number of parameters, one may assume that the motor only unbinds from the (DD) state with $i = 7$ as shown in Fig. 7(b). Furthermore, for small values of $F$, the unbinding rate $\omega_{\mathrm{off}}$ of kinesin is of the order of 1/s whereas the transition rates between the different bound states $i = 1, 2, \ldots, 7$ are of the order of or larger than 1/(10 ms). This separation of time scales implies that the kinesin motor has essentially attained the steady state of the 7-state network before it starts to undergo transitions from the bound state $i = 7$ to the unbound state $i = 0$ provided the load force $F$ is sufficiently small. Its unbinding rate can then be estimated by[19]

$$\omega_{\mathrm{off}} \simeq P_7^{\mathrm{st}} \omega_{70} = P_7^{\mathrm{st}} \kappa_{70} \exp(F/F_{\mathrm{d},7}) = P_7^{\mathrm{st}} \kappa_{70} \exp(\chi_{70} \bar{F}). \tag{2.27}$$

This unbinding rate depends on the load force $F$ both via the explicit exponential factor and via the occupation probability $P_7^{\mathrm{st}} = P_7^{\mathrm{st}}(F)$. Comparison with relation (2.24) then leads to the zero-force unbinding rate

$$\kappa_{\mathrm{off}} \simeq P_7^{\mathrm{st}}(0) \kappa_{70}. \tag{2.28}$$

Likewise, the overall detachment force $F_{\mathrm{d}}$ in (2.24) will, in general, differ from $F_{\mathrm{d},7}$ because of the force dependence of $P_7^{\mathrm{st}}$.

The average run time $\langle \Delta t \rangle$ should decrease monotonically with increasing $F$ and vanishes in the limit of large $F$. In contrast, the average run length $\langle \Delta x \rangle = v \langle \Delta t \rangle$ vanishes already at the stall force $F = F_{\mathrm{s}}$, at which the motor velocity $v$ changes sign, compare Fig. 8.

For kinesin, the $F$-dependence of the run length is displayed in Fig. 11(a) where the experimental data of Ref. 23 are compared with calculations based on the chemomechanical network in Fig. 7(b) as described in Ref. 19. The latter calculations lead to the zero-force unbinding rate $\kappa_{70} \simeq 3/\mathrm{s}$ and to the parameter $\chi_{70} = 0.1$, which implies the detachment force $F_{\mathrm{d},7} = k_B T/\ell \chi_{70} \simeq 5\,\mathrm{pN}$ at room temperature. On the other hand, if the data in Fig. 11(a) are directly fitted as $\langle \Delta x \rangle \sim \exp(-F/F_{\mathrm{d}})$, one obtains the overall detachment force $F_{\mathrm{d}} \simeq 3\,\mathrm{pN}$ as deduced in Ref. 23.

For the 7-state network in Fig. 7(b), the zero-force unbinding rate $\kappa_{\mathrm{off}}$ as given by (2.28) is proportional to the steady state probability $P_7^{\mathrm{st}}$ that the motor occupies the (DD) state. Inspection of Fig. 7(b) shows that this occupation probability decreases as one increases the ATP concentration since one then decreases the flux from state

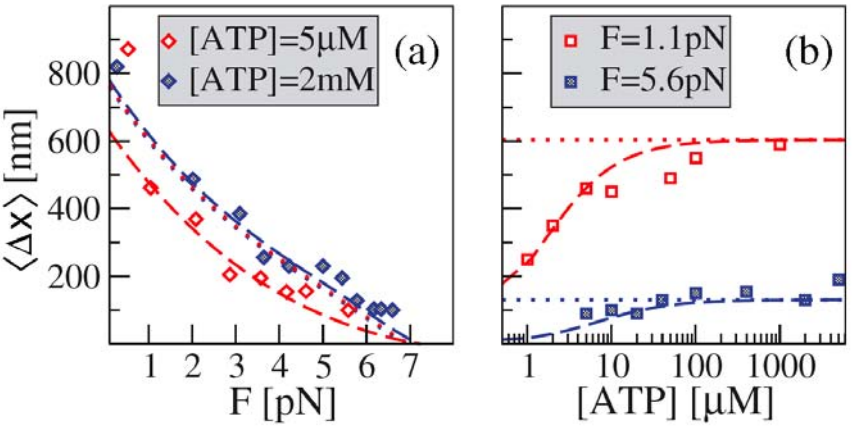


Fig. 11. Average run length (or walking distance) $\langle \Delta x \rangle$ of kinesin as a function (a) of load force $F$ and (b) of ATP concentration. With increasing $F$, the run length first decays by an exponential factor that is governed by the detachment force $F_{\rm d}$ and then vanishes at the stall force $F = F_{\rm s}$, compare Fig. 8. The experimenal data are from Ref. 23, the broken lines represent the behavior as calculated in Ref. 19 for the network in Fig. 7(b). These latter calculations lead to the detachment force $F_{d,7} \simeq 5$ pN while a simple exponential fit to the data implies $F_{\rm d} \simeq 3$ pN as explained in the text.

(DE) with $i = 1$ to state (DD) with $i = 7$ relative to the flux from state (DE) to state (DT) with $i = 2$. For the same reason, the probability $P_7^{\rm st}$ also decreases if one decreases the ADP concentration. Thus, the 7-state model in Fig. 7(b) predicts that the zero-force unbinding rate $\kappa_{\rm off}$ depends on the nucleotide concentrations.

In order to check the assumed separation of time scales, one may consider the unbinding process as another 'absorption' process with only one absorbing state given by $i = 0$. If the motor starts in the initial state $i = a$, the probability distribution for the process to exhibit the run time $s \equiv \Delta t$ is given by

$$\rho_{a|0}^{\rm ab}(s) = \frac{\partial}{\partial s} P_{a0}(s) = P_{a7}(s)\omega_{70}, \tag{2.29}$$

compare relation (2.20). Now, let $P_a^{\rm in}$ be the probability that the motor is initially in state $i = a$. The probability distribution for the run time $s$ is then given by

$$\rho_0^{\rm ab}(s) = \sum_{a \neq 0} P_a^{\rm in} P_{a7}(s)\omega_{70}, \tag{2.30}$$

and the average run time $\langle \Delta t \rangle$ is equal to the first moment of this distribution.

## 3. Composite Walks of Single Motors

### 3.1. *Directed walks interrupted by diffusive motion*

Now, let us follow the movements of a single motor on length scales that exceed its run length $\Delta x$. The motor then undergoes composite walks, which consist of directed movements along the filaments interrupted by periods of random, diffusive

motion in the surrounding solution. In this section, we will discuss these motor walks for the dilute transport regime of small motor concentration, for which the bound motors do not 'feel' each other. As shown in Sec. 3.2.2 below, for single motors without cargo, this dilute regime corresponds to a situation, in which the motor's run length is smaller than the average separation of the bound motors. For single motors that pull a cargo particle of lateral extension $\ell_{\rm ca} \gg \ell$, the dilute concentration regime is further reduced by a factor $\ell/\ell_{\rm ca}$.

The main features of composite walks by single motors or by cargo particles pulled by a single motor can be understood from the following, simple scaling argument.[27] After placed onto a filament, a single motor steps along this filament up to its run time $\Delta t$, at which it unbinds. On time scales that are large compared to this run time, the probability $P_{\rm b}$ to find the motor bound to the filament will decay to zero. This probability can be estimated if one focusses on the diffusive motion in the $d_\perp$ directions perpendicular to the filament as described by the perpendicular position vector $\vec{r}_\perp$. This diffusion is governed by the Gaussian distribution

$$\mathcal{P}_{\rm Ga}(\vec{r}_\perp) = (4\pi D_{\rm ub} t)^{-d_\perp/2} \exp(-\vec{r}_\perp^{\,2}/4D_{\rm ub}t) \tag{3.1}$$

with the diffusion constant $D_{\rm ub}$ for the unbound motor state. The bound state probability $P_{\rm b}$ can then be estimated by the probability that the diffusive motor returns to the filament at $\vec{r}_\perp = 0$ which leads to

$$P_{\rm b} \sim \mathcal{P}_{\rm Ga}(\vec{r}_\perp = \vec{0}) \sim 1/t^{-d_\perp/2}. \tag{3.2}$$

In the bound state, the motor has the average velocity $v$; in the unbound state, its average velocity is zero. The effective transport velocity of the motor parallel to the filament is then given by

$$v_{\rm eff} = vP_{\rm b} \sim 1/t^{-d_\perp/2} \tag{3.3}$$

which decays to zero as $1/t^{1/2}$ in two dimensions and as $1/t$ in three dimensions. Therefore, the motor displacement parallel to the filament is proportional to $t^{1/2}$ in two dimensions and to $\ln(t)$ in three dimensions.[e]

In order to describe these composite walks in a quantitative way, we will now define their properties in terms of the single motor parameters as obtained in the previous section.

## 3.2. *Parameter mapping for motor walks*

### 3.2.1. *Continuous-time walks and transition rates*

In Sec. 2.3, the chemomechanical coupling of stepping motors has been discussed in terms of discrete motor states, that are distinguished by the chemical composition

[e]The 3-dimensional case is a boundary case; in higher dimensions with $d_\perp > 2$, the motor has a finite probability that it never returns to the filament, and the average displacement of the motor parallel to the filament is equal to zero.

of their catalytic motor domains. For kinesin, the corresponding chemomechanical networks are displayed in Fig. 7. Some of these motor states are again shown in Fig. 12(a), which illustrates a single mechanical step along the lattice of filament binding sites.

Since we now want to describe the movement of the motor on length scales that are large compared to the step size $\ell = 8\,\mathrm{nm}$, we introduce a reduced description and replace the motor molecule by a walker that steps along the lattice of binding sites with certain transition rates as shown in Fig. 12(b). When the motor dwells in a certain binding site, it can make a forward step with rate $\omega_\mathrm{f}$, a backward step with rate $\omega_\mathrm{b}$, and unbinds from the filament with rate $\omega_\mathrm{off}$.[f] These rates can be determined from experimentally accessible quantities.

As explained in the previous section, the unbinding rate $\omega_\mathrm{off}$ is identical with the inverse run time $1/\langle \Delta t \rangle$, see (2.22). The forward and backward stepping rates $\omega_\mathrm{f}$ and $\omega_\mathrm{b}$ are related to the motor velocity $v$ and to the ratio $q$ of forward to backward steps, compare Fig. 8, according to

$$v = \ell(\omega_\mathrm{f} - \omega_\mathrm{b}) \quad \text{and} \quad q = \omega_\mathrm{f}/\omega_\mathrm{b} \tag{3.4}$$

which implies

$$\omega_\mathrm{f} = \frac{1}{1 - 1/q}\frac{v}{\ell} \quad \text{and} \quad \omega_\mathrm{b} = \frac{1}{q - 1}\frac{v}{\ell}. \tag{3.5}$$

Note that these expressions do not contain any singularity for $q = 1$ since this value corresponds to the stall force $F = F_\mathrm{s}$, at which the velocity $v$ vanishes as well, see

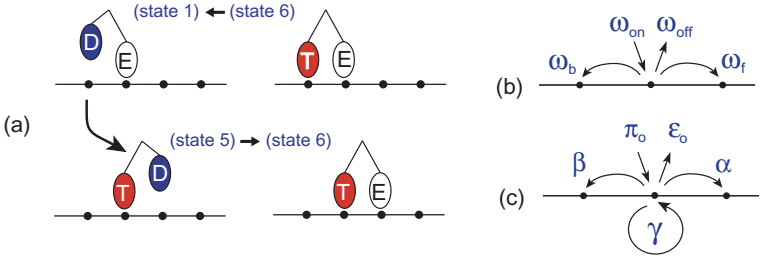


Fig. 12. (a) One forward step of two-headed kinesin along the lattice of binding sites provided by one protofilament. Each step involves several motor states; for simplicity, only the states $i = 1, 5$ and 6 of the networks in Figs. 7(b) and 7(c) are displayed. As explained in Figs. 7, the catalytic site of each head can be empty (E), contain one ATP molecule (T), or one ADP molecule (D). The forward step occurs between state 1 and state 5; (b) Continuous-time walk with forward stepping rate $\omega_\mathrm{f}$, unbinding rate $\omega_\mathrm{off}$, binding rate $\omega_\mathrm{on} = \kappa_\mathrm{on} C$, and backward stepping rate $\omega_\mathrm{b}$; and (c) Discrete-time walk with forward stepping probability $\alpha$, unbinding probability $\epsilon_o$, binding probability $\pi_o$, backward probability $\beta$, and dwell probability $\gamma$.[27]

[f]In Ref. 7, the rate $\omega_\mathrm{off}$ has been denoted by $\bar{\epsilon}_o$.

Fig. 8. If the stepping dynamics is described by a Markov process, the average dwell time $\tau_{\rm dw}$ of the motor at a certain filament site is then given by

$$\tau_{\rm dw} = \frac{1}{\omega_{\rm f} + \omega_{\rm b} + \omega_{\rm off}}. \tag{3.6}$$

Finally, unbound motors that diffuse in the surrounding solution can bind to an unoccupied filament site. The corresponding binding rate $\omega_{\rm on}$, which is equal to the number of motors that bind to a single filament site per unit time, depends on the molar concentration $C$ of the unbound motors. In order to discuss this binding rate, let us consider a system with volume $V$ that contains a certain number of filament binding sites $N_{\rm si}$ and a certain number of motors $N_{\rm mo} = N_{\rm b} + N_{\rm ub}$ where $N_{\rm b}$ and $N_{\rm ub}$ represent the average number of bound and unbound motors, respectively. We then obtain the molar concentration

$$C \equiv N_{\rm ub}/N_{\rm Av}V \tag{3.7}$$

of the motors with Avogadro's number $N_{\rm Av} \simeq 6 \times 10^{23}$ (assuming that the filament volume can be neglected) and the binding ratio

$$n_{\rm b} \equiv N_{\rm b}/N_{\rm si}. \tag{3.8}$$

The dissociation constant $C_{\rm dis}$ is then defined by the relation

$$n_{\rm b} \approx C/C_{\rm dis} \quad \text{for small } C. \tag{3.9}$$

For molar concentrations $C \gtrsim C_{\rm dis}$, the binding ratio $n_{\rm b} \lesssim 1$ and the binding sites of the filaments are more or less covered by motors. For kinesin, e.g., the dissociation constant $C_{\rm dis} \simeq 100\,{\rm nM}$ for typical in vitro assays. This molar concentration corresponds to an average motor-motor separation of about 255 nm within such an assay. This implies that the filaments become already overcrowded with kinesin motors for a rather dilute bulk concentration of this motor.

The dependence of the binding rate $\omega_{\rm on}$ on the molar concentration $C$ is now described by

$$\omega_{\rm on} \approx \kappa_{\rm on} C \quad \text{for small } C, \tag{3.10}$$

which defines the binding rate constant $\kappa_{\rm on}$. In the steady state, the binding flux $\omega_{\rm on}$ must balance the unbinding flux $\omega_{\rm off} n_{\rm b}$. Using the asymptotic relations (3.10) and (3.9), this flux balance equation becoms

$$\omega_{\rm on} \approx \kappa_{\rm on} C \approx \omega_{\rm off} n_{\rm b} \approx \omega_{\rm off} C/C_{\rm dis} \tag{3.11}$$

for small $C$ which implies that the binding rate constant $\kappa_{\rm on}$ is given by

$$\kappa_{\rm on} = \frac{\omega_{\rm off}}{C_{\rm dis}} = \frac{1}{\langle \Delta t \rangle C_{\rm dis}}. \tag{3.12}$$

Since the unbinding rate $\omega_{\rm off}$ as given by (2.24) depends on the load force $F$, so does the product $\kappa_{\rm on} C_{\rm dis}$.

For large ATP concentration and low load force, kinesin is characterized by the run time $\langle \Delta t \rangle \simeq 1\,{\rm s}$, the velocity $v \simeq 800\,{\rm nm/s}$, and the dissociation constant $C_{\rm dis} \simeq$

100 nM. The relations (2.22), (3.5), (3.12) then lead to the zero-force unbinding rate $\kappa_{\rm off} \simeq 1/{\rm s}$, the forward stepping rate $\omega_{\rm f} \simeq 100/{\rm s}$, and the binding rate constant $\kappa_{\rm on} \simeq 10/(\mu{\rm M\ s})$.

### 3.2.2. *Dilute transport regime*

We can now give a precise definition of the dilute transport regime in which even the bound motors can be treated as noninteracting particles. Let us consider the general situation, in which the bound motor covers or occupies $\ell_{\rm mo}/\ell$ binding sites. The ratio $\ell_{\rm mo}/\ell$ should typically assume a value between $\ell_{\rm mo}/\ell = 1$ for single-site occupancy and $\ell_{\rm mo}/\ell = 2$ for two-site occupancy by the motor. In all cases, the ratio $\ell_{\rm mo}/\ell$ should be of order one.

If these motors are bound to the filaments with binding ratio $n_{\rm b}$, the probability $\rho_{\rm b}$ that a single binding site is occupied by a motor is then given by

$$\rho_{\rm b} = (\ell_{\rm mo}/\ell) n_{\rm b} \approx \ell_{\rm mo} C/\ell C_{\rm dis} \tag{3.13}$$

where the definition of the dissociation constant $C_{\rm dis}$ as given by (3.9) has been used. The probability that the motor can reach the next binding site in the forward direction is then $(1-\rho_{\rm b})$ which is also equal to the probability that the motor can make a forward step without bumping into another bound motor. Therefore, the probability that the motor can make $\langle \Delta x\rangle/\ell$ successive steps without interactions with other bound motors is given by $(1-\rho_{\rm b})^{\langle \Delta x\rangle/\ell} \approx \exp[-\langle \Delta x\rangle \rho_{\rm b}/\ell]$. The dilute transport regime is defined by the criterion that this latter probability is close to one which implies the inequality

$$\rho_{\rm b} \ll \ell/\langle \Delta x\rangle \tag{3.14}$$

for the single-site occupation probability $\rho_{\rm b}$. It then follows from (3.13) that the molar concentration $C$ of the motors should belong to the concentration regime defined by

$$C \ll \frac{\ell}{\ell_{\rm mo}} \frac{\ell}{\langle \Delta x\rangle} C_{\rm dis}. \tag{3.15}$$

Alternatively, we may consider the average separation $\langle L_{\rm b,b}\rangle = \ell/n_{\rm b}$ of the bound motors. The inequality (3.14) then implies that the dilute transport regime corresponds to

$$\langle L_{\rm b,b}\rangle \gg (\ell_{\rm mo}/\ell)\langle \Delta x\rangle. \tag{3.16}$$

Since the ratio $\ell_{\rm mo}/\ell \gtrsim 1$, the dilute transport regime for a single motor without cargo is also defined by the criterion that the average separation $\langle L_{\rm b,b}\rangle$ of the bound motors is large compared to their run length $\langle \Delta x\rangle$.

This line of arguments can be easily generalized to the situation of cargo particles pulled by single motors. In this case, the relation (3.9) still applies provided $C$, $C_{\rm dis}$, and $n_{\rm b}$ now denote the molar concentration, dissociation constant, and binding ratio of the cargo particles. If these cargo particles cover $\ell_{\rm ca}/\ell$ binding sites of the

filament with $\ell_{\rm ca}/\ell > \ell_{\rm mo}/\ell$, the single site occupation probability $\rho_{\rm b}$ is now given by $\rho_{\rm b} = (\ell_{\rm ca}/\ell)n_{\rm b}$. It then follows from the inequality (3.14) for $\rho_{\rm b}$ that the dilute transport regime of cargo particles pulled by a single motor corresponds to the regime

$$C \ll \frac{\ell}{\ell_{\rm ca}} \frac{\ell}{\langle \Delta x \rangle} C_{\rm dis} \tag{3.17}$$

for the molar concentration of these cargo particles. The cargo size $\ell_{\rm ca}$ can be much larger than the step size $\ell$ which implies that the dilute concentration regime can be strongly reduced by the factor $\ell/\ell_{\rm ca}$.

### 3.2.3. *Discrete-time walks and transition probabilities*

In order to study the motor walks by stochastic simulations, it is convenient to use discrete-time random walks which are defined by the time scale $\tau_o$ of an elementary time step[g] and by the transition probabilities as shown in Fig. 12(c).[27,28,37] Within one time step, the motor makes a forward step with probability $\alpha$, a backward step with probability $\beta$, and unbinds from the filament with unbinding probability $\epsilon_o$; in addition, it can simply dwell at the same binding site with dwell probability $\gamma$. These probabilities satisfy the normalization condition $\alpha + \beta + \gamma + \epsilon_o = 1$.

The unbinding probability $\epsilon_o$ is related to the unbinding rate $\omega_{\rm off}$ via

$$\epsilon_o = \frac{\omega_{\rm off}\tau_o}{1 + \omega_{\rm off}\tau_o} \quad \text{or} \quad \omega_{\rm off} = \frac{\epsilon_o}{1-\epsilon_o}\frac{1}{\tau_o}. \tag{3.18}$$

The forward and backward stepping probabilities $\alpha$ and $\beta$ satisfy

$$\alpha = \frac{\omega_{\rm f}\tau_o}{1 + \omega_{\rm off}\tau_o} \quad \text{or} \quad \omega_{\rm f} = \frac{\alpha}{1-\epsilon_o}\frac{1}{\tau_o} \tag{3.19}$$

and

$$\beta = \frac{\omega_{\rm b}\tau_o}{1 + \omega_{\rm off}\tau_o} \quad \text{or} \quad \omega_{\rm b} = \frac{\beta}{1-\epsilon_o}\frac{1}{\tau_o}. \tag{3.20}$$

The definition of the average dwell time $\tau_{\rm dw}$ as given by (3.6) together with the normalization condition $\alpha + \beta + \epsilon_o = 1 - \gamma$ then imply the relation

$$\tau_{\rm dw} = \frac{(1-\epsilon_o)\tau_o}{1-\gamma} \quad \text{or} \quad \gamma = 1 - (1-\epsilon_o)\frac{\tau_o}{\tau_{\rm dw}}. \tag{3.21}$$

After the motor has detached from the filament, it undergoes undirected diffusive motion in the surrounding solution. This diffusive motion can be described in the framework of lattice walks as introduced in Ref. 27. The properties of these walks can be solved analytically for the simplest system geometries[28,67] and can be studied by mean field theory and simulations for more complex systems.[27,37,68]

[g]In Refs. 27 and 37, the time scale of the elementary time step was denoted by $\tau_{\rm b}$ and $\tau$, respectively. In fact, somewhat different parameter mappings were used in these two studies as explained in App. C of Ref. 6.

Alternatively, one may also study continuous diffusion in the unbound state as in Ref. 69. For the lattice walks studied in Refs. 27, 28, and 37, the binding probability $\pi_o$ was taken to be $\pi_o = 2\pi_{\rm ad}/3$ where $\pi_{\rm ad}/6$ is the probability that the motor walker binds to a certain filament site from a neighboring site on a simple cubic lattice. The binding current or flux onto a single filament site is then given by $\pi_o \rho_{\rm ub}$ where $\rho_{\rm ub}$ is the volume fraction of the motor heads defined by

$$\rho_{\rm ub} \equiv N_{\rm ub} c_{\rm he} \ell^3 / V = c_{\rm he} \ell^3 N_{\rm Av} C \tag{3.22}$$

with a dimensionless coefficient $c_{\rm he}$ of order one and the molar motor concentration $C$ as in (3.7).[h] The asymptotic relation

$$(\pi_o/\tau_o)\rho_{\rm ub} \approx \kappa_{\rm on} C \quad \text{for small } C \tag{3.23}$$

then leads to the binding probability

$$\pi_o = \kappa_{\rm on} \tau_o C / \rho_{\rm ub} = \kappa_{\rm on} \tau_o / c_{\rm he} \ell^3 N_{\rm Av}. \tag{3.24}$$

In the simulations, the time scale $\tau_o$ of the elementary time step is chosen in such a way that the dimensionless unbinding rate $\omega_{\rm off}\tau_o \ll 1$. It then follows from (3.18) that $\epsilon_o \approx \omega_{\rm off}\tau_o$ which leads to the ratio

$$\frac{\epsilon_o}{\pi_o} \approx \frac{\omega_{\rm off}}{\kappa_{\rm on}} c_{\rm he} \ell^3 N_{\rm Av} \tag{3.25}$$

of the transition probabilities $\epsilon_o$ and $\pi_o$. For kinesin with $\omega_{\rm off} = 1/{\rm s}$, $\kappa_{\rm on} = 10/(\mu{\rm M\ s})$, and $\ell = 8\,{\rm nm}$, one obtains $\epsilon_o/\pi_o \simeq 0.6 \times 10^{-5}$ for $c_{\rm he} = 2$.

A more detailed description of the motor walks takes the nonexponential dwell time distributions for the mechanical steps[20] into account, as briefly described in Sec. 2.3.6 above. Alternatively, one may study walks, for which the motors can attain several internal states at each binding site.[70] In the dilute regime, this refinement does not affect the large scale properties of the composite walks. In contrast, the internal motor dynamics does have observable effects on the traffic of mutually exclusive motors.[70]

### 3.3. *Composite motor walks in two and three dimensions*

The simplest systems in which one can study composite motor walks are provided by single filaments in unbounded geometries, i.e., without confining walls. In this case, one can use Fourier-Laplace transforms of the 2- and 3-dimensional lattice models in order to obtain analytical solutions for many quantities of interest.[28,67] These explicit solutions confirm the simple scaling behavior in (3.3) and extend the results as obtained by similar scaling arguments in Ref. 27.

Instead of a single motor, let us consider the equivalent situation of an ensemble of noninteracting motors with a probability distribution that is initially localized

[h]For kinesin, the two heads are separated by a distance of order $\ell$, which implies that both heads occupy a volume $c_{\rm he}\ell^3$ with $c_{\rm he} \simeq 2$.

at a single filament site. This initial distribution evolves with time into two distinct distributions, one for the bound motors, the other for the unbound motors. Both distributions are shifted in the forward direction parallel to the filament. For the bound motors, this leads to the average displacement shown in Fig. 13(a). In addition, the stochastic nature of the motor movements leads to a broadening of both the bound and the unbound motor distributions. This broadening can be characterized by the variance of the motor displacements as shown in Fig. 13(b) for the bound motors. In both Figs. 13(a) and 13(b), the analytical results are in excellent agreement with Monte Carlo data.

The instantaneous diffusion coefficient $D_b$ of the bound motors parallel to the filament is given by the slope of the variance shown in Fig. 13(b). For large times, this diffusion coefficient attains anomalously large values in two dimensions and exhibits large logarithmic correction terms in three dimensions. Very similar behavior is found for the diffusion of the unbound motors parallel to the filament. In addition, the diffusion is anisotropic since the perpendicular diffusion coefficients are smaller than the parallel ones. Therefore, the probability distributions for the unbound and bound motors are elongated parallel to the filament and are compressed perpendicular to it.[28,67]

### 3.4. *Composite walks within compartments*

The asymptotic behavior of the composite motor walks depends on the geometry of the compartment in which the motors move. In bead motility assays, one usually considers filaments that are immobilized on the walls of large compartments as shown in Fig. 14(a) and (b) which correspond to a half space and to a slab geometry, respectively. Another interesting geometry is provided by tube-like compartments as in Fig. 14(c)–14(e) which represent primitive models for axons.

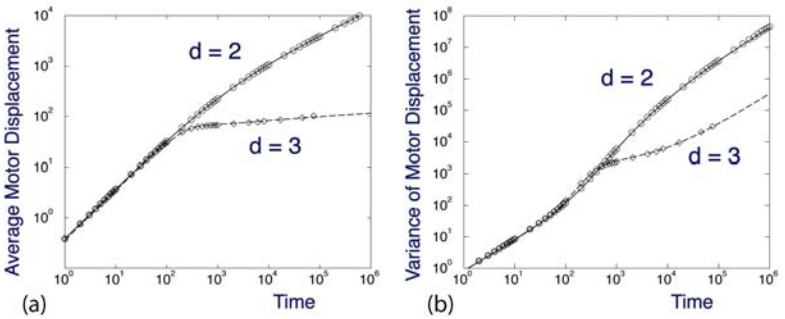


Fig. 13. Composite motor walks in two and three dimensions: (a) Average displacement of bound motors parallel to the filament; and (b) Variance of displacements of bound motors in units of the step size $\ell$ as functions of time in units of the elementary time step $\tau_o$. The slope of the variance in (b) defines the effective diffusion coefficient $D_{\rm b}$ which is anomalously large. In both plots, the curves represent analytical results for d = 2 and d = 3 dimensions whereas the data represent the results of Monte Carlo simulations.[28]

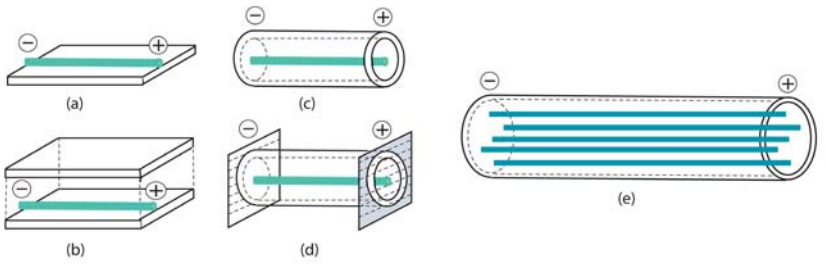


Fig. 14. Different compartment geometries with filaments (green lines): (a) Half space geometry and (b) Slab geometry with a single filament immobilized on the walls of these compartments; (c,d) Tube-like compartments with (c) open and (d) closed orifices enclosing a single, freely suspended filament; and (e) Tube-like compartment with many parallel and unipolar filaments. The plus and minus signs indicate the plus and minus ends of the filaments.

In all of these compartments, the effective motor velocity $v_{\rm eff}$ decays with time $t$ as soon as $t$ exceeds the run time $\langle \Delta t \rangle$, see Fig. 15. In the half space, the effective motor velocity $v_{\rm eff}$ exhibits the same power law decay $\sim 1/t$ as predicted by the simple scaling relation (3.3) for three dimensions. In the slab geometry, the effective velocity first decreases as in the half space until the motor feels the other wall of the slab at time $t = \Delta t_\perp$. For longer times, the decay of the effective velocity follows the power law $\sim 1/t^{1/2}$ as predicted by the simple scaling relation (3.3) for two dimensions. For an open tube, the effective velocity is reduced by a constant factor, which depends on the radius of the tube.[27]

In order to estimate the reduction of the effective velocity in a tube-like compartment, let us consider such a compartment with length $L$ and cross-sectional area $A_{\rm cr}$. The compartment contains a dilute solution with $N_{\rm mo}$ motors and several parallel filaments with $N_{\rm pr}$ accessible protofilaments, as indicated in Fig. 14(b), which implies $N_{\rm si} = N_{\rm pr}(L/\ell)$ binding sites. In order to suppress effects from the two ends of the tube, it is convenient to use periodic boundary conditions, which could be experimentally realized by a torus-shaped tube. We then attain a steady state with an average number of bound motors, $N_{\rm b}$, and binding ratio $n_{\rm b} = N_{\rm b}/N_{\rm si} \approx C/C_{\rm dis}$ for small $C$ as in (3.9). Using the relations $N_{\rm mo} = N_{\rm b} + N_{\rm ub} = N_{\rm si} n_{\rm b} + VCN_{\rm Av} \approx (N_{\rm si} + VC_{\rm dis}N_{\rm Av})n_{\rm b}$ that follow from the definitions of binding ratio $n_{\rm b}$ and molar concentration $C$, one obtains the bound state probability

$$P_{\rm b} = N_{\rm b}/N_{\rm mo} \approx 1/(1 + C_{\rm dis}N_{\rm Av}\ell A_{\rm cr}/N_{\rm pr}). \tag{3.26}$$

Furthermore, in the dilute regime with $C \ll C_{\rm dis}\ell/\langle \Delta x \rangle$, we can ignore any interactions between the bound motors and take the bound state velocity to be equal to the single motor velocity $v$. Therefore, the effective velocity of a single motor parallel to the tube is now given by[27,37]

$$v_{\rm eff} = vP_{\rm b} = v/(1 + C_{\rm dis}N_{\rm Av}\ell A_{\rm cr}/N_{\rm pr}) \tag{3.27}$$

which explicitly shows the reduction of the effective motor velocity by motor unbinding since the dissocation constant $C_{\rm dis} = \omega_{\rm off}/\kappa_{\rm on}$ is inversely proportional to the

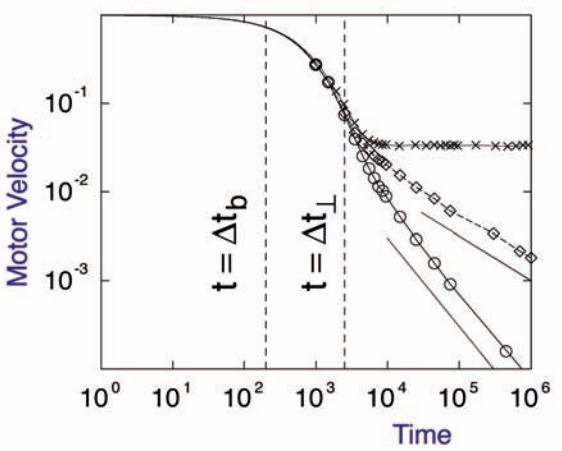


Fig. 15. Effective motor velocity $v_{\rm eff}$ parallel to the filament as a function of time for the half space (circles), slab (diamonds), and tube geometry (crosses). Time is measured in units of the elementary time scale $\tau_o$, velocity in units of $\ell/\tau_o$ with step size $\ell$. Up to the run time $t = \langle \Delta t \rangle$, the motors walk along the filament with the motor velocity $v$ of the bound motor. The intermediate time regime up to $t = \Delta t_\perp$ is characterized by diffusive excursions, which are small compared to the thickness of the slab or the diameter of the tube. Finally, for large $t$, the effective velocity decays as $1/t$ and $1/t^{1/2}$ for the half space and the slab, respectively, but attains a constant value for the tube.[27]

run time $\langle \Delta t \rangle$, see (3.12). Therefore, the effective motor velocity $v_{\rm eff}$ attains its maximal value, which is equal to the velocity $v$ of the bound motor, in the limit of large run times.

### 3.5. *Active diffusion in slab-like compartments*

So far, we have focussed on compartments containing single filaments or a group of parallel and isopolar filaments as in Fig. 14. In general, one can use different types of filament patterns in order to induce different types of motor movements. In particular, one may use slab-like compartments with crossed filament patterns as shown in Fig. 16 in order to enhance the diffusion of the motors and their cargo.[29] For the pattern in Fig. 16(a), several filaments with random orientation are located in each surface stripe. For the pattern in Fig. 16(b), all filaments have the same orientation within one surface stripe but neighboring stripes have opposite orientation. Such filament patterns can be constructed, e.g., by using chemically or topographically structured surface domains covered by inactive motors or other chemical crosslinkers.[71–77] Another interesting method is provided by microfabricated surface pillars, to which the filaments can be attached.[78]

For the systems shown in Fig. 16, the motor and its cargo undergo non-directed but enhanced diffusion. The effective diffusion constant $D_{\rm eff}$ is primarily determined by the competition of two length scales: the mesh size, say $L_\perp$, of the filament pattern and the average run length $\langle \Delta x \rangle$ of the motors.[29] If the mesh size exceeds

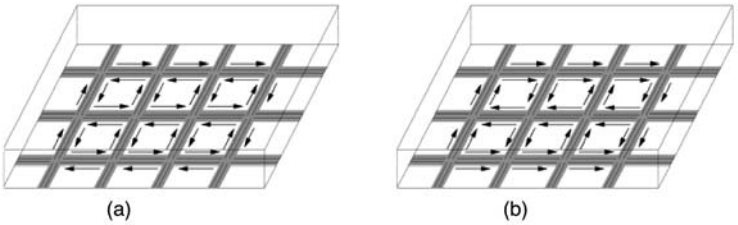


Fig. 16. Different patterns of filaments that lead to active and enhanced diffusion of motors: (a) Striped surface domains, each of which contains immobilized filaments with both orientations; and (b) Striped surface domains, for which all filaments within one stripe have the same orientation but neighboring stripes have opposite orientation. The arrows indicate the direction of walking motors.

the run length, i.e., for $\langle \Delta x \rangle < L_\perp$, the effective diffusion constant behaves as $D_{\text{eff}} \sim v\langle \Delta x \rangle$. On the other hand, if the run length exceeds the mesh size, i.e., for $\langle \Delta x \rangle > L_\perp$, the diffusion constant is governed by the mesh size and one has $D_{\text{eff}} \sim L_\perp v$ which corresponds to a random walk with effective step size $L_\perp$ and effective step time $L_\perp/v$.

For a cargo particle in solution, the unbound diffusion constant is inversely proportional to the linear cargo size $R$ because of Stokes friction arising from the viscosity of the solution. In contrast, the effective diffusion constant for the active diffusion of molecular motors is hardly affected by the viscosity of the solution and, thus, is rather insensitive to the size of the cargo particle. Therefore, for micrometer-sized cargo particles in water, this effective diffusion constant for active diffusion can exceed the unbound diffusion constant by several orders of magnitude.[29]

For a given type of motor, the maximal value for the effective diffusion constant $D_{\text{eff}}$ is $D_{\text{eff}} \sim v\langle \Delta x \rangle$. Thus, in order to increase this coefficient, one must either increase the bound state velocity $v$ or the run length $\langle \Delta x \rangle$ of the motors. One rather effective way to increase the run length is to use cooperative transport of cargo by several motors as discussed in the next section.

## 4. Cargo Transport by Teams of Molecular Motors

In vivo, stepping motors are responsible for the intracellular transport of various types of cargo particles such as vesicles, organelles, and filaments. This cargo transport is typically performed by *several* motor molecules as revealed by electron microscopy[79,80] and single particle tracking.[81–84] In some cases, the transport is uni-directional as one would expect if all motors that pull on the cargo belong to the same motor species. In many cases, the cargo moves in a bi-directional manner, however, which implies that it is pulled by two antagonistic motor teams corresponding to two different motor species.

In Sec. 4.1, we discuss uni-directional transport of a single cargo particle by one team of $N$ identical motors. Compared to the behavior of a single motor, such a

cargo particle exhibits a run length that increases rather strongly with $N$ and an apparant stall force that increases sublinearly with $N$.

In Sec. 4.2, bi-directional transport of a single cargo particle is considered, in which this particle is pulled by two teams of plus and minus motors. The two motor teams perform a stochastic tug-of-war that is characterized by strongly fluctuating forces acting on each motor arising from the force balance between the two teams. As a result, one finds seven distinct motility regimes, which are determined by the numbers $N_+$ and $N_-$ of plus and minus motors as well as by the single motor parameters. All available experimental data on bi-directional cargo transport can be understood in terms of such a tug-of-war.

### 4.1. *Uni-directional transport by one motor species*

Now, consider a single cargo particle with $N$ motors, which are firmly attached to this particle, see Fig. 17. When in contact with the filament, each motor has a finite run length and run time which implies that the actual number $n$ of pulling motors is not constant but varies with time between zero and $N$. Thus, if we include the unbound state with $n = 0$, the cargo can be in $N+1$ different states $(n)$, which are distinguished by the number $n$ of active pulling motors.

If the cargo is in state $(n)$, the binding of one motor to the filament leads to state $(n+1)$ and the unbinding of one motor from the filament to state $(n-1)$. The transition from state $(n)$ to state $(n-1)$ occurs with unbinding rate $\omega_{n,n-1}$, the transition from $(n)$ to $(n+1)$ with binding rate $\omega_{n,n+1}$. The probabilities $P_n = P_n(t)$ that the cargo particle is in state $(n)$ at time $t$ then evolve according to the master equation[30]

$$\frac{\partial}{\partial t} P_n = -\Delta J_{n,n+1} - \Delta J_{n,n-1} \tag{4.1}$$

with

$$\Delta J_{n,n+1} \equiv P_n \omega_{n,n+1} - P_{n+1} \omega_{n+1,n} \tag{4.2}$$

and

$$\Delta J_{n,n-1} \equiv P_n \omega_{n,n-1} - P_{n-1} \omega_{n-1,n}. \tag{4.3}$$

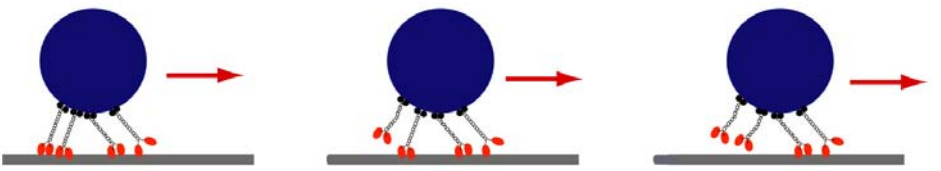

Fig. 17. Uni-directional transport of a cargo particle by $N = 4$ identical motors. The motors are firmly attached to the particle but unbind from and rebind to the filament. Therefore, the actual number $n$ of pulling motors varies with time between $n = 0$ and $n = N$.

In the steady state, the probability distribution $P_n = P_n^{\rm st}$ satisfies

$$P_{n+1}^{\rm st}\omega_{n+1,n} = P_n^{\rm st}\omega_{n,n+1} \tag{4.4}$$

for $0 \leq n \leq N-1$. This relation corresponds to detailed balance between the states $(n+1)$ and $(n)$ and reflects the fact that all movements of the bound cargo particle begin and end with $n = 0$ and that every transition from $(n)$ to $(n+1)$ implies a backward transition at some later time. It is also implicitly assumed here that the binding and unbinding rates are independent of the transition rates for stepping along the filament.

In vivo, the pulling motors are attached to their cargo via a long and flexible stalk. In addition, electron micrographs indicate that the spacing of the motors on the cargo is comparable to their length. We now focus on such a 'dilute' regime, in which the motors do not interfere with each other apart from the fact that they are attached to the same cargo. In this case, the transition rates $\omega_{n,n-1}$ and $\omega_{n,n+1}$, have the simple form[30]

$$\omega_{n,n-1} = n\omega_{\rm off} \quad \text{and} \quad \omega_{n,n+1} = (N-n)\omega_{\rm on} \tag{4.5}$$

where the combinatorial factors $n$ and $N-n$ arise from the different possibilities to unbind or bind a motor when the cargo particle is in state $(n)$. The unbinding rate $\omega_{\rm off}$ is taken to be equal to the unbinding of a *single* motor as given by (2.22).[i] The binding rate $\omega_{\rm on}$, on the other hand, reflects the effective motor concentration, $C_{\rm eff}$, between the cargo particle and the filament. Thus, the binding rate of a single motor attached to the cargo should have the form

$$\omega_{\rm on} = \kappa_{\rm on} C_{\rm eff}. \tag{4.6}$$

As mentioned, kinesin is characterized by the unbinding rate $\omega_{\rm off} \simeq 1/{\rm s}$ and the binding rate constant $\kappa_{\rm on} \simeq 10/(\mu{\rm M\,s})$. In Ref. 30, we used the estimate $\omega_{\rm on} = 5/{\rm s}$ for kinesin as suggested by experiments[45] in which the motors pull membrane tubes. This value for the binding rate $\omega_{\rm on}$ corresponds to an effective molar concentration $C_{\rm eff} \simeq 0.5\,\mu{\rm M}$ or an average separation between the motors of about 150 nm.

### 4.1.1. *Regime of low load force*

As emphasized before, the number of pulling motors changes with time in a stochastic manner. It is then instructive to consider the average number $\langle n \rangle$ of pulling motors where the average is taken over all bound states of the motor. If the cargo particle does not experience a load force or, more generally, if this load force is sufficiently small, this average number can be calculated explicitly for noninterfering

[i]Strictly speaking, the unbinding motor heads always experience some constraints arising from the attachment of the other end of the motor to the cargo particle. These constraints will be ignored here.

motors. If the cargo particle is initially bound to the filament by a single motor, i.e., $n(t=0)=1$ , one obtains the expression[30]

$$\langle n\rangle = \frac{1}{1+k_{\rm off}}\frac{(1+k_{\rm off})^N}{(1+k_{\rm off})^N - k_{\rm off}^N}N \le N \tag{4.7}$$

which depends on the maximal motor number $N$ and on the dimensionless desorption coefficient for zero force as given by

$$k_{\rm off} \equiv \omega_{\rm off}(F=0)/\omega_{\rm on} = \omega_{\rm off}/\kappa_{\rm on}C_{\rm eff} = C_{\rm dis}/C_{\rm eff} \tag{4.8}$$

with the motor's dissociation constant $C_{\rm dis}$ as defined in (3.9). Since the average in (4.7) is taken over the bound states of the cargo particle, one has $1 \le \langle n\rangle \le N$; the limiting values $\langle n\rangle = 1$ and $\langle n\rangle = N$ are attained for large and small $k_{\rm off}$, respectively. Furthermore, the relation (4.7) leads to $\langle n\rangle \approx N/(1+k_{\rm off})$ for large $N$.

When the noninterfering motors pull on the cargo in the absence of load, they move with their single motor velocity $v$. Thus, in this situation, the cargo particle also has velocity $v_{\rm ca} = v$ for all cargo states $(n)$. The average run length $\langle \Delta x_{\rm ca}\rangle$ of the cargo particle is then given by[30]

$$\langle \Delta x_{\rm ca}\rangle \approx (v/\omega_{\rm off}N)(1/k_{\rm off})^{N-1} \tag{4.9}$$

and the correspondig unbinding rate by

$$\omega_{\rm off,ca} = v/\langle \Delta x_{\rm ca}\rangle \approx \omega_{\rm off}Nk_{\rm off}^{N-1} \tag{4.10}$$

for small zero-force desorption coefficient $k_{\rm off} = \omega_{\rm off}/\omega_{\rm on} \ll 1$, i.e., for strongly binding motors. Thus, in this case, the run length increases exponentially and the unbinding rate decreases exponentially with increasing number of motors. It is interesting to note that the two relations (4.9) and (4.10) are also valid for a cargo particle with $N=1$ and then reduce to $\langle \Delta x_{\rm ca}\rangle = \langle \Delta x\rangle$ and $\omega_{\rm off,ca} = \omega_{\rm off}$. If the cargo is pulled by up to $N$ kinesin motors with $k_{\rm off} \simeq 0.2$, the expression as given by (4.9) leads to the estimate $\langle \Delta x_{\rm ca}\rangle \simeq 5^{N-1}/N\,\mu$m which implies that $N=7$ or $N=8$ kinesin molecules are sufficient to attain an average run length in the centimeter range.

### 4.1.2. *Run length distributions*

In addition to the average value $\langle \Delta x_{\rm ca}\rangle$ of the run length, the model described in the previous subsection can also be used to calculate the full run length distribution $\Psi(\Delta x_{\rm ca})$,[30] which develops a 'fat' tail for $N>1$ as shown in Fig. 18. In this figure, the theoretical distributions are compared with experimental ones that have been obtained in vitro by preparing carboxylated polystyrene beads covered with kinesin.[32] In order to vary the motor coverage of the beads, the mass density $c$ of the kinesin molecules in the incubation chamber is changed for fixed bead concentration. The coverage increases linearly over a certain mass density range until saturation

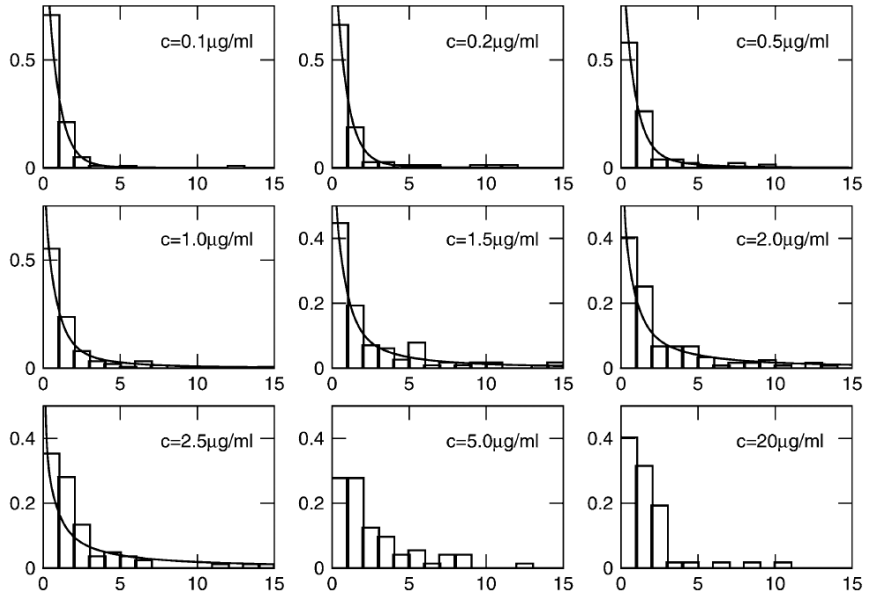


Fig. 18. Run length distributions $\Psi(\Delta x_{\rm ca})$ of cargo particles that have been incubated at different mass densities $c$ of kinesin. In each panel, the columns represent the experimental data, and the full lines the theoretical curves as obtained from (4.16). The seven curves for the mass densities $0.1\mu{\rm g/ml} \leq c \leq 2.5\mu{\rm g/ml}$ have been obtained using the density scale $c_o = 0.79\mu{\rm g/ml}$ and the binding rate $\omega_{\rm on} = 5.1/{\rm s}$. This implies that the average number $\langle n\rangle$ of pulling motors increases from $\langle n\rangle = 1.1$ for $c = 0.1\mu{\rm g/ml}$ to $\langle n\rangle = 3.2$ for $c = 2.5\mu{\rm g/ml}$. For concentrations $c$ that are comparable to or larger than $5\mu{\rm g/ml}$, the linear relation (4.12) between $\langle N\rangle$ and $c$ is no longer fulfilled.[32]

is reached as deduced from dynamic light scattering experiments. The maximal coverage is estimated to be about 130 motors per bead.

When a bead prepared in this way is brought into contact with immobilized microtubules, only a relatively small fraction of the attached motors can pull simultaneously on the bead. The maximal number of motors that can do so corresponds to the number $N$ as defined for a single cargo particle in the previous subsection. Because of the used preparation method, this number varies from bead to bead. Thus, if one observes a large number $\mathcal{N}_{\rm bea}$ of different beads, the behavior of this ensemble of cargo particles involves the additional distribution $P_{\rm bea}(N)$ for the number $N$. The simplest choice for $P_{\rm bea}(N)$ is a Poisson distribution

$$\mathcal{P}_{\rm Po}(N) \equiv \frac{(c/c_o)^N e^{-c/c_o}}{N!} \tag{4.11}$$

which leads to the average number

$$\langle N\rangle = c/c_o \tag{4.12}$$

where the density scale $c_o$ is used as a fit parameter and obtained from the detailed comparision between theory and experiment, see Fig. 18. Since the average number

$\langle N \rangle$ turns out to be relatively small, it is convenient to use the truncated Poisson distribution as given by[32]

$$P_{\rm bea}(N) = \frac{1}{Z}\mathcal{P}_{\rm Po}(N) \quad \text{for} \quad 1 \leq N \leq N_{\rm max} \tag{4.13}$$

with the normalization constant

$$Z \equiv \sum_{N=1}^{N_{\rm max}} \mathcal{P}_{\rm Po}(N). \tag{4.14}$$

The maximal number $N_{\rm max}$ is chosen in such a way that all $\mathcal{N}_{\rm bea}$ beads, for which the run length is determined in the experiments, are likely to have $N \leq N_{\rm max}$ motors attached to them. This condition can be ensured by

$$\mathcal{N}_{\rm bea}\frac{\mathcal{P}_{\rm Po}(N_{\rm max})}{(1-\mathcal{P}_{\rm Po}(0))} \geq 1 \quad \text{and} \quad \mathcal{N}_{\rm bea}\frac{\mathcal{P}_{\rm Po}(N_{\rm max}+1)}{(1-\mathcal{P}_{\rm Po}(0))} < 1. \tag{4.15}$$

The theoretical run length distributions $\Psi(\Delta x_{\rm ca})$ as shown in Fig. 18 have been obtained by first calculating the run length distributions $\Psi_N(\Delta x_{\rm ca})$ for each $N \leq N_{\rm max}$ and then taking the average over $N$ which leads to

$$\Psi(\Delta x_{\rm ca}) = \sum_{N=1}^{N_{\rm max}} P_{\rm bea}(N)\Psi_N(\Delta x_{\rm ca}). \tag{4.16}$$

These theoretical distributions were fitted to seven experimental distributions using only two fit parameters, namely the density scale $c_o$ and the binding rate $\omega_{\rm on}$. The best fit was obtained for $c_o = 0.79\mu$g/ml and $\omega_{\rm on} = 5.1$/s, see Fig. 18.

As a result, the maximal motor number $N_{\rm max}$ is found to vary between $N_{\rm max} = 2$ and $N_{\rm max} = 7$ for mass densities $c$ between $0.1\mu$g/ml and $2.5\mu$g/ml corresponding to molar concentrations between 0.27 and 6.7 nM. In the same concentration range, the average number $\langle n \rangle$ of pulling motors is found to lie between $\langle n \rangle = 1.1$ and $\langle n \rangle = 3.2$ motors.

All distributions $\Psi(\Delta x_{\rm ca})$ in Fig. 18 decrease monotonically with increasing run length $\Delta x_{\rm ca}$. Such a monotonic decay is expected since these run length distributions were obtained for beads that bind after diffusing towards the filaments. Indeed, such a deposition method implies that the beads are initially connected to the filaments by a single motor molecule corresponding to the initial condition $P_n(t=0) = \delta_{n,1}$.[30,32] Recently, a run length distribution has been reported for which all runs exceeded a minimal length of $6\mu$m.[31] The motility assay used in this latter study was similar to the one in Ref. 32 but the deposition of the kinesin-coated beads onto the microtubules was performed by optical tweezers. In the concentration regime, in which the bead carries several motors, this deposition method is likely to lead to an initial state of the bound bead, in which this bead is connected to the microtubule by several motors. In such a situation, the run length distribution can develop a maximum but this maximum is expected to lie at a run length below $6\mu$m.

A more direct comparison between theory and experiment would be possible if one prepared cargo particles with a precise number $N > 1$ of motors attached to each of them. One appealing approach consists in crosslinker molecules, each of which binds $N > 1$ motors. One could then study the attachment of these crosslinkers in the dilute limit, in which the cargo particle carries at most one crosslinker. So far, such a preparation method has not been developed.

### 4.1.3. *Force dependence of uni-directional transport*

If the cargo particle does not experience a load force, noninterfering motors unbind and rebind in a statistically independent manner. In contrast, in the presence of such a force, even noninterfering motors become coupled via the cargo. If the cargo is subject to the force $F$, the $n$ active motors share this force, and each single motor feels the reduced force

$$F_1 \equiv F/n \tag{4.17}$$

which now depends on $n$. Since $n$ changes with time in a stochastic manner, so does the force $F_1$ acting on each motor. In order to understand the consequence of this coupling between the motors, one has to take the force dependence of the different transition rates into account.

The unbinding rate $\omega_{\rm off}$ of a *single* motor increases exponentially with the load force $F$, see (2.24). Thus, a single motor that experiences the load force $F_1 = F/n$ unbinds from the filament with unbinding rate $\omega_{\rm off} = \kappa_{\rm off} \exp(F/nF_{\rm d})$ where $F_{\rm d}$ denotes the detachment force of a single motor as before. It then follows from (4.5) that the transition rate from cargo state $(n)$ to state $(n-1)$ is given by

$$\omega_{n,n-1} = \omega_{\rm off}(n) = n\kappa_{\rm off} e^{F_1/F_{\rm d}} = n\kappa_{\rm off} e^{F/nF_{\rm d}}. \tag{4.18}$$

Thus, all unbinding rates increase exponentially with increasing load and the corresponding force scale $nF_{\rm d}$ depends on the number $n$ of pulling motors.

As long as the cargo particle is bound to the filament, i.e., for $n \geq 1$, the effective motor concentration $C_{\rm eff}$ between the cargo and the filament, which enters the binding rate $\omega_{\rm on}$ of a single motor attached to the cargo, see (4.6), cannot be substantially reduced by the load force $F$. The simplest assumption that is consistent with this constraint is to consider the force-independent binding rate

$$\omega_{n,n+1} = \omega_{\rm on}(n) = (N-n)\kappa_{\rm on} C_{\rm eff}(F=0) = (N-n)\omega_{\rm on}, \tag{4.19}$$

compare (4.6).

For noninterfering motors as considered here, the steady state probabilities $P_n^{\rm st}$ to find the cargo particle in state $(n)$ are now given by the explicit expression

$$P_n^{\rm st} = \left(\frac{1}{k_{\rm off}}\right)^n e^{-H_n F/F_{\rm d}} \binom{N}{n} P_0^{\rm st} \tag{4.20}$$

with the zero-force desorption coefficient $k_{\rm off}$ as in (4.8), the harmonic numbers

$$H_n \equiv \sum_{m=1}^{n} \frac{1}{m}, \tag{4.21}$$

the binomial coefficient $\binom{N}{n}$, and the normalization condition

$$P_0^{\rm st} + \sum_{n=1}^{N} P_n^{\rm st} = 1 \tag{4.22}$$

as follows from (4.4).[j] Since the harmonic numbers $H_n$ satisfy the inequalities $c_{\rm Eu} + \ln(n) < H_n \leq 1 + \ln(n)$ with Euler's constant $c_{\rm Eu} \simeq 0.577$, the second factor in (4.20) behaves as

$$e^{-H_n F/F_{\rm d}} \sim 1/n^{F/F_{\rm d}} \tag{4.23}$$

as a function of $n$.

Because the noninterfering motors interact only via their common cargo, the steady state probabilities $P^{\rm st}$ depend only on the detachment force $F_{\rm d}$ but not on the stall force $F_{\rm s}$, which characterizes the force-velocity relationship of a single motor. In general, this relationship can be written as

$$v = \mathcal{V}(F) \quad \text{with } \mathcal{V}(F = F_{\rm s}) = 0 \tag{4.24}$$

where $\mathcal{V}(F)$ is a monotonically decreasing function of $F$ between $0 \leq F \leq F_{\rm s}$, compare Fig. 8(a). Since the force acting on the cargo particle is equally shared by the $n$ pulling motors, they all experience the same force $F_1 = F/n$ and, thus, have the same velocity equal to the instantaneous cargo velocity

$$v_{{\rm ca},n}(F) = \mathcal{V}(F/n) = \mathcal{V}(F_1). \tag{4.25}$$

As a pulling motor unbinds from the filament, the force acting on a single motor increases from $F_1 = F/n$ to $F_1 = F/(n-1)$ and the instanteneous cargo velocity decreases from $\mathcal{V}(F/n)$ to $\mathcal{V}(F/(n-1))$. Likewise, as a detached motor rebinds to the filament, the instanteneous velocity increases from $\mathcal{V}(F/n)$ to $\mathcal{V}(F/(n+1))$. In the steady state, the average cargo velocity $v_{\rm ca}$ is then given by

$$v_{\rm ca}(F) = \sum_{n=1}^{N} P_n^{\rm st} v_{{\rm ca},n}(F) \sim \sum_{n=1}^{N} \left(\frac{1}{k_{\rm off}}\right)^n \frac{1}{n^{F/F_{\rm d}}} \binom{N}{n} \mathcal{V}(F/n) \tag{4.26}$$

where the $n$-independent factor $P_0 \leq 1$ has been omitted in the second relation. With increasing load force $F$, each term in the sum decreases because of (i) the factor $1/n^{F/F_{\rm d}}$ and (ii) the reduction of the instantaneous velocity $\mathcal{V}(F/n)$. For $n \leq F/F_{\rm s}$, the instantaneous velocity $\mathcal{V}(F/n)$ is small and vanishes if one ignores

[j] For $F = 0$, the probability $P_0^{\rm st}$ for the unbound state is given by $P_0^{\rm st} = 1/(1 + \omega_{\rm on}/\omega_{\rm off})^N$.

backward steps.[k] Thus, for $F > mF_s$, only cargo states ($n$) with $n > m$ contribute significantly to the sum in (4.26), and their contribution is reduced by the factor $1/n^{F/F_d} < 1/m^{F/F_d}$. As a result, the cargo velocity seems to vanish at an apparent stall force $\hat{F}_{s,N}$, which is smaller than the true stall $F_{s,N} \equiv NF_s$. For kinesin with $k_{off} = 0.2$ and $F_s = 6\,\mathrm{pN}$, for example, one finds $\hat{F}_{s,5} \simeq 20\,\mathrm{pN}$ and $F_{s,5} = 30\,\mathrm{pN}$ as well as $\hat{F}_{s,10} \simeq 30\,\mathrm{pN}$ and $F_{s,10} = 60\,\mathrm{pN}$.[30] Therefore, the apparent stall force $\hat{F}_{s,N}$, which may be viewed as the force generated by the team of $N$ motors, increases with $N$ but is substantially smaller than $F_{s,N} = NF_s$ for large $N$.

In Ref. 30, both the average cargo velocity $v_{ca}(F)$ and the probability distribution for the instantaneous velocity of the cargo have been calculated for kinesin with $k_{off} \simeq 0.2$. With increasing load, the latter distribution is shifted towards smaller velocity values, becomes broader, and develops several peaks in agreement with recent experimental observations[82–84] on the in vivo transport of vesicles and organelles.

### 4.2. *Bi-directional transport by two motor species*

In biological cells, the motion of cargo particles along microtubules is often observed to be bi-directional in the sense that the particle frequently switches its direction of motion. Since both kinesin and dynein motors are bound to these particles, it is rather natural to assume that the bi-directional motion arises from the competition between these two motor species. The molecular mechanism underlying this competition has been controversial for some time.

Two scenarios have been discussed:[33,34] (i) Tug-of-war between two motor teams: Each motor species tries to move the cargo into its own direction, thereby performing a tug-of-war on the cargo as illustrated in Fig. 19; and (ii) Coordination by a putative protein complex: Such a complex could prevent opposing motors from being active at the same time, thereby excluding state (0) in Fig. 19. The observed complexity of bidirectional transport has led many authors to reject a tug-of-war scenario and to search for a coordination complex. However, as recently shown in Ref. 35, this conclusion was premature because the *stochastic* nature of a realistic tug-of-war leads to rather complex transport behavior as observed experimentally.

Thus, let us consider a team of plus and a team of minus motors that pull in opposite directions; the direction of instantaneous motion is determined by the stronger team as in the two states (+) and (−) of Fig. 19. However, since the number of motors that actually pull varies with time in a stochastic manner for both motor species, the weaker team may suddenly become the stronger one which reverses the direction of motion. Indeed, because of the stochastic unbinding and rebinding of the motors, each individual motor experiences a strongly fluctuating load force. The instanteneous value of this force depends both on the number of

[k]If one takes backward steps into account, the terms with $n < F/F_s$ give a small and negative contribution to the sum in (4.26).

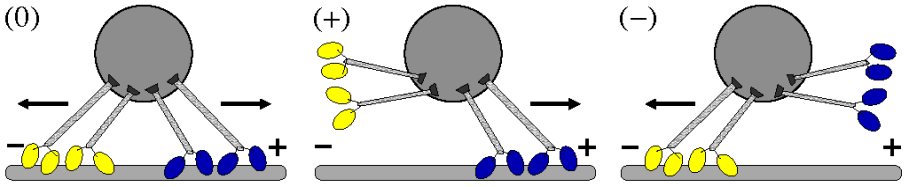


Fig. 19. Cargo transport by 2 plus (blue) and 2 minus (yellow) motors: possible configurations (0), (+), and (−) of motors bound to the microtubule. For configuration (0), the motors block each other so that the cargo does not move. For configuration (+) and (−), the cargo exhibits fast plus and minus motion, respectively.[35]

motors that pull in the opposite direction and on the number of motors that pull in the same direction since the latter number determines how many motors share the force generated by the opposing team.

### 4.2.1. *Single motor properties and sign conventions*

In order to describe the movements of both motor species in a consistent manner, we have to be careful about the signs of their velocities and the signs of the forces experienced by them. We will use the convention that (i) the velocity of a plus motor is positive in the absence of force, which implies that the zero-force velocity of a minus motor is negative; and (ii) a load force $F$ is positive if it acts against the forward direction of the plus motors which is identical to the backward direction of the minus motors. Both conventions have also been used in the previous sections for the plus motor kinesin. In addition, we will also take the detachment and stall forces of both motor species to be positive.

Each motor species is now characterized by its force-dependent unbinding rate $\omega_{\rm off}$, which defines the detachment force $F_{\rm d}$ as in (2.24), its binding rate constant $\kappa_{\rm on}$ as in (3.10) and (3.12), and its force-velocity relationship as in (4.24), which involves the stall force $F_{\rm s}$. Thus, if a single *plus* motor feels the load force $F = F_{1+} > 0$, its unbinding rate is given by

$$\omega_{\rm off,+} = \kappa_{\rm off,+} e^{F_{1+}/F_{\rm d,+}} \tag{4.27}$$

which depends on the detachment force $F_{\rm d,+}$ of this motor. The binding rate of each plus motor is taken to be

$$\omega_{\rm on,+} = \kappa_{\rm on,+} C_{+,\rm eff} \tag{4.28}$$

where $C_{+,\rm eff}$ denotes the effective molar concentration of the plus motors between the cargo particle and the filament, again assumed to be independent of load force. Furthermore, the force-velocity relationship of the plus motors is now given by

$$\begin{aligned} v_+ &= \mathcal{V}_+(F_{1+}) > 0 \quad \text{for } F_{1+} < F_{\rm s,+} \\ &= \mathcal{V}_+(F_{1+}) < 0 \quad \text{for } F_{1+} > F_{\rm s,+} \end{aligned} \tag{4.29}$$

with their stall force $F_{\rm s,+}$ defined by

$$\mathcal{V}_+(F_{1+} = F_{\rm s,+}) = 0. \tag{4.30}$$

If the *minus* motors feel a load force $F = F_{1-} < 0$, they are characterized by the unbinding rate

$$\omega_{\mathrm{off},-} = \kappa_{\mathrm{off},-} e^{|F_{1-}|/F_{\mathrm{d},-}}, \tag{4.31}$$

which involves the corresponding detachment force $F_{\mathrm{d},-}$. The binding rate of a single minus motor is also taken to be force-independent and given by

$$\omega_{\mathrm{on},-} = \kappa_{\mathrm{on},-} C_{-,\mathrm{eff}} \tag{4.32}$$

with the effective concentration $C_{-,\mathrm{eff}}$ of minus motors between the cargo particle and the filament. Finally, the minus motors are characterized by the force-velocity relationship

$$\begin{aligned} v_- &= \mathcal{V}_-(|F_{1-}|) < 0 \quad \text{for } |F_{1-}| < F_{\mathrm{s},-} \\ &= \mathcal{V}_-(|F_{1-}|) > 0 \quad \text{for } |F_{1-}| > F_{\mathrm{s},-}, \end{aligned} \tag{4.33}$$

and the implicit equation

$$\mathcal{V}_-(|F_{1-}| = F_{\mathrm{s},-}) = 0 \tag{4.34}$$

for the stall force $F_{\mathrm{s},-}$.

It is important to emphasize that almost all of these parameters can be determined from a systematic analysis of experimental data. For the plus motor kinesin, for example, the zero-force unbinding rate $\kappa_{\mathrm{off},+} \simeq 1/\mathrm{s}$, the detachment force $F_{\mathrm{d},+} \simeq 3 - 5\,\mathrm{pN}$, the binding rate constant $\kappa_{\mathrm{on},+} \simeq 10/(\mu\mathrm{M\,s})$, and the stall force $F_{\mathrm{s},+} \simeq 6 - 7\,\mathrm{pN}$ as mentioned before. The only quantities that are difficult to measure directly are the effective molar concentrations $C_{+,\mathrm{eff}}$ and $C_{-,\mathrm{eff}}$.

### 4.2.2. *Stochastic tug-of-war*

The stochastic tug-of-war between the plus and minus motors can be described by an appropriate generalization of the model as given by (4.1) to the case of two motor species. The cargo particle now carries $N_+$ plus motors and $N_-$ minus motors, and the cargo can attain $(N_+ + 1)(N_- + 1)$ states $(n_+, n_-)$ which are characterized by the actual numbers $n_+$ and $n_-$ of plus and minus motors that pull at the same time. These states form a square lattice as shown in Fig. 20.

When the cargo particle dwells in state $(n_+, n_-)$, it can undergo up to four different transitions. The unbinding of a plus motor from this state is governed by the rate

$$\omega(n_+, n_-|n_+ - 1, n_-) \equiv \omega_{\mathrm{off},+}(n_+, n_-) = n_+ \kappa_{\mathrm{off},+} e^{F_{1+}/F_{\mathrm{d},+}}, \tag{4.35}$$

the unbinding of a minus motor by the rate

$$\omega(n_+, n_-|n_+, n_- - 1) \equiv \omega_{\mathrm{off},-}(n_+, n_-) = n_- \kappa_{\mathrm{off},-} e^{|F_{1-}|/F_{\mathrm{d},-}}. \tag{4.36}$$

In addition, the binding rates of a plus and a minus motor are equal to

$$\omega(n_+, n_-|n_+ + 1, n_-) \equiv \omega_{\mathrm{on},+}(n_+, n_-) = (N_+ - n_+)\omega_{\mathrm{on},+} \tag{4.37}$$

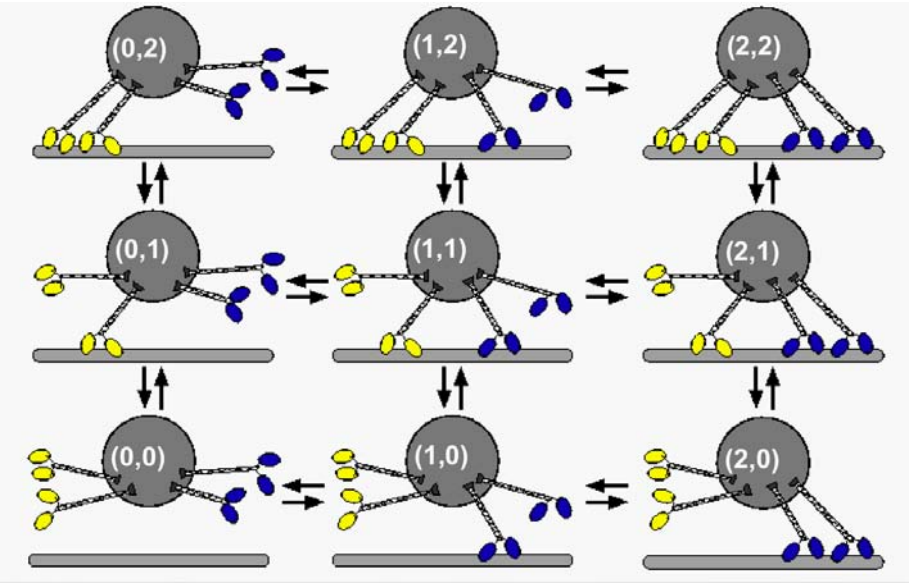


Fig. 20. State space of cargo with $N_+ = 2$ plus and $N_- = 2$ minus motors. The $(N_+ + 1)(N_- + 1)$ states are labeled by $(n_+, n_-)$ corresponding to $n_+$ plus (blue) and $n_-$ minus (yellow) motors, that simultaneously pull on the cargo. These states form a square lattice with $0 \leq n_+ \leq N_+$ and $0 \leq n_- \leq N_-$.

and

$$\omega(n_+, n_-|n_+, n_- + 1) \equiv \omega_{\mathrm{on},-}(n_+, n_-) = (N_- - n_-)\omega_{\mathrm{on},-}. \tag{4.38}$$

So far, the two unbinding rates in (4.35) and (4.36) have been expressed in terms of the two forces $F_{1+}$ and $F_{1-}$ experienced by a single plus and minus motor. It is important to note, however, that these two forces are not independent of each other, but are strongly coupled during cargo transport as soon as both motor species are active, i.e., as soon as both $n_+ > 0$ and $n_- > 0$. This can be understood from the force balance explained in the next subsection.

### 4.2.3. *Force balance between two motor species*

Thus, let us consider a cargo state $(n_+, n_-)$ with $n_+ > 0$ and $n_- > 0$. The forces experienced by a single plus and a single minus motor are denoted by $F_{1+}$ and $F_{1-}$ as before. The total force experienced by the $n_+$ plus motors is then equal to

$$F_{n+} = n_+ F_{1+} > 0. \tag{4.39}$$

Likewise, the total force experienced by the minus motors is

$$F_{n-} = n_- F_{1-} < 0. \tag{4.40}$$

In the absence of an external load force, Newton's third law implies that[1]

$$F_{n+} = |F_{n-}| \quad \text{or} \quad n_- F_{1+} = n_+ |F_{1-}|. \tag{4.41}$$

For a given state $(n_+, n_-)$, one can distinguish three cases depending on the relative size of $n_+ F_{\mathrm{s},+}$ and $n_- F_{\mathrm{s},-}$. The first case with $n_+ F_{\mathrm{s},+} > n_- F_{\mathrm{s},-}$ corresponds to plus motor dominance. Likewise, the second case with $n_- F_{\mathrm{s},-} > n_+ F_{\mathrm{s},+}$ describes minus motor dominance. Both cases are smoothly connected by the special case with $n_- F_{\mathrm{s},-} = n_+ F_{\mathrm{s},+}$.

For *plus motor dominance* with $n_+ F_{\mathrm{s},+} > n_- F_{\mathrm{s},-}$, the plus motors step forward if a single plus motor experiences the load force $F_{1+} < F_{\mathrm{s},+}$ which implies that the $n_+$ plus motors feel the load $F_{n+} = n_+ F_{1+} < n_+ F_{\mathrm{s},+}$. In addition, the minus motors step backward if a single minus motor experiences the load force $|F_{1-}| > F_{\mathrm{s},-}$ and the $n_-$ minus motors feel the load $|F_{n-}| = n_- |F_{1-}| > n_- F_{\mathrm{s},-}$. Because of the relation $F_{n+} = |F_{n-}|$ as given by (4.41), these two inequalities can be combined into

$$n_- F_{\mathrm{s},-} < F_{n+} = |F_{n-}| < n_+ F_{\mathrm{s},+} \tag{4.42}$$

which is a necessary condition for forward steps of the plus motors and backward steps of the minus motors. For *minus motor dominance* with $n_- F_{\mathrm{s},-} > n_+ F_{\mathrm{s},+}$, the same kind of reasoning leads to the expression

$$n_+ F_{\mathrm{s},-} < F_{n+} = |F_{n-}| < n_- F_{\mathrm{s},-} \tag{4.43}$$

which is a necessary condition for forward steps by the minus motors and backward steps of the plus motors. The two conditions (4.42) and (4.43) can now be combined into the general condition

$$\min(n_+ F_{\mathrm{s},+}, n_- F_{\mathrm{s},-}) \le F_{n+} = |F_{n-}| \le \max(n_+ F_{\mathrm{s},+}, n_- F_{\mathrm{s},-}) \tag{4.44}$$

where the equalities include the special case with $n_+ F_{\mathrm{s},+} = n_- F_{\mathrm{s},-}$.

The two inequalities in (4.44) imply that the force $F_{n+}$ experienced by the $n_+$ plus motors can be expressed as

$$F_{n+} = (1-\lambda) n_- F_{\mathrm{s},-} + \lambda n_+ F_{\mathrm{s},+} \quad \text{with} \quad 0 < \lambda < 1. \tag{4.45}$$

What remains to be done is to determine the parameter $\lambda$. This can be achieved by matching the instantaneous velocities of the plus and minus motors.

[1]In the presence of an external load force $F_{\mathrm{ex}}$, the force balance becomes $F_{n+} = |F_{n-}| + F_{\mathrm{ex}}$.

### 4.2.4. *Matching of instantaneous velocities*

When the cargo particle is in state $(n_+, n_-)$, its instantaneous velocity $v_{\rm ca}(n_+, n_-)$ must be equal to the instanteneous velocities of both the plus motors and the minus motors, which implies

$$v_{\rm ca}(n_+, n_-) = \mathcal{V}_+(F_{1+}) = \mathcal{V}_-(|F_{1-}|). \tag{4.46}$$

The second equality is equivalent to the implicit equation

$$\mathcal{V}_+(F_{n+}/n_+) = \mathcal{V}_-(F_{n+}/n_-) \tag{4.47}$$

for the force $F_{n+}$ where the force balance equation $|F_{n-}| = n_-|F_{1-}| = F_{n+}$ has been used again. If $F_{n+}$ is expressed in terms of the parameter $\lambda$ as in (4.45), the matching condition (4.47) becomes an implicit equation for this parameter.

The matching condition $\mathcal{V}_+(F_{n+}/n_+) = \mathcal{V}_-(F_{n+}/n_-)$ can be solved graphically. In order to do so, one has to plot the two rescaled force-velocity relationships $\mathcal{V}_+(F_{n+}/n_+)$ and $\mathcal{V}_-(F_{n+}/n_-)$ as a function of $F_{n+}$. An example for such a graphical solution is shown in Fig. 21 for the cargo state $(n_+, n_-) = (3, 2)$ and for piece-wise linear force-velocity relationships. In the latter case, one may also obtain an explicit relation for the parameter $\lambda$, see Ref. 35.

In this way, one can determine the total load force $F_{n+} = F_{n+}(n_+, n_-)$ experienced by the $n_+$ plus motors for all cargo states $(n_+, n_-)$. The force $F_{n+}$ can then be used to calculate the forces $F_{1+} = F_{n+}/n_+$ and $|F_{1-}| = F_{n+}/n_-$ as experienced

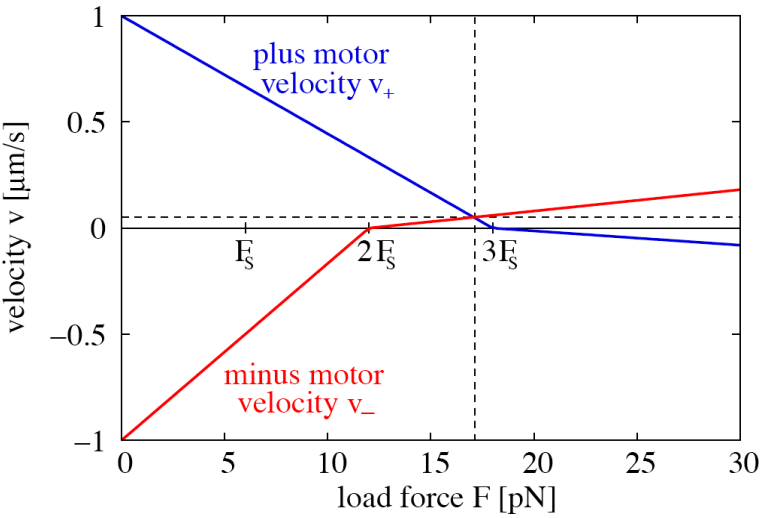


Fig. 21. Graphical solution of the matching condition (4.47) for the instantaneous cargo velocity $v = v_{\rm ca}(n_+, n_-)$ and the total load force $F = F_{n+}$ experienced by the $n_+$ plus motors in state $(n_+, n_-) = (3, 2)$ with $F_{n+} = |F_{n-}|$. Both the force-velocity relationship $v_+ = \mathcal{V}_+(F/n_+)$ for the plus motors (blue lines) and the corresponding relationship $v_- = \mathcal{V}_-(F/n_-)$ for the minus motors (red lines) have been taken to be piece-wise linear. The intersection point of these two functions determines the cargo velocity $v = v_{\rm ca}(n_+, n_-)$ and the total load force $F = F_{n+}$ as indicated by the broken lines.

by a single plus and minus motor, respectively. When these expressions are inserted into the relations (4.35) and (4.36), one obtains the rate

$$\omega_{\mathrm{off},+}(n_+,n_-) = n_+\kappa_{\mathrm{off},+}e^{F_{n+}(n_+,n_-)/n_+F_{\mathrm{d},+}}, \tag{4.48}$$

for the unbinding of one plus motor from state $(n_+,n_-)$ and the corresponding rate

$$\omega_{\mathrm{off},-}(n_+,n_-) = n_-\kappa_{\mathrm{off},-}e^{F_{n+}(n_+,n_-)/n_-F_{\mathrm{d},-}} \tag{4.49}$$

for the unbinding of one minus motor. These two expressions show explicitly that these unbinding rates provide a direct coupling between the motor numbers $n_+$ and $n_-$.

### 4.2.5. *Different motility states of cargo particles*

The stochastic tug-of-war model described in the previous subsections leads to rather complex dynamic behavior related to seven different motility states. These motility states can be distinguished by the qualitative shape of the steady state distributions $P^{\mathrm{st}}(n_+,n_-)$ for the two motor numbers $n_+$ and $n_-$. First, there are three different states for which the distribution $P^{\mathrm{st}}(n_+,n_-)$ has a *single maximum*. This single maximum may be located at the boundaries of the $(n_+,n_-)$-plane with $(n_+,n_-) = (n,0)$ or $(n_+,n_-) = (0,n)$, compare Fig. 20. These states represent fast plus directed or minus directed motion. Alternatively, this maximum may be located away from the boundaries of the $(n_+,n_-)$-plane and then corresponds to a state with a strongly reduced cargo velocity as determined by the velocity of the backward stepping motors. In particular, when it is located along the diagonal of the $(n_+,n_-)$-plane with $n_+ = n_-$ or $n_+ = n_- \pm 1$, the maximum represents a 'no motion' state, in which the two motor species block each other and the cargo particle exhibits, on average, no directed motion.

Second, the cargo can attain three different motility states for which the distribution $P^{\mathrm{st}}(n_+,n_-)$ has *two local maxima*. Both of these maxima may be located at the boundaries of the $(n_+,n_-)$-plane and then lead to the switching between fast plus directed and fast minus directed motion, i.e., to bi-directional transport without pauses. In addition, the distribution $P^{\mathrm{st}}(n_+,n_-)$ may have one maximum away from the boundary of the cargo's state space and one maximum at this boundary. These latter distributions represent uni-directional transport in the plus or minus direction interrupted by prolonged pauses (or strongly reduced transport). Finally, the distribution $P^{\mathrm{st}}(n_+,n_-)$ may exhibit *three local maxima* corresponding to bi-directional transport interrupted by pauses.

As one changes the single motor parameters and/or the motor numbers $N_+$ and $N_-$, the system may undergo a transition from one motility state to another. The most important single motor parameters that determine the cargo's motility state are the two desorption coefficients

$$k_{\mathrm{off},+} \equiv \frac{\kappa_{\mathrm{off},+}}{\omega_{\mathrm{on},+}} \quad \text{and} \quad k_{\mathrm{off},-} \equiv \frac{\kappa_{\mathrm{off},-}}{\omega_{\mathrm{on},-}} \tag{4.50}$$

as well as the force ratios

$$f_+ \equiv \frac{F_{\mathrm{s},+}}{F_{\mathrm{d},+}}, f_- \equiv \frac{F_{\mathrm{s},-}}{F_{\mathrm{d},-}} \quad \text{and} \quad f_{\mathrm{s}} \equiv \frac{F_{\mathrm{s},+}}{F_{\mathrm{s},-}}. \tag{4.51}$$

4.2.6. *Motility states for symmetric tug-of-war*

A particularly instructive case is provided by a 'symmetric' tug-of-war that is defined by the following two simplifying features: (i) Equal numbers of plus and minus motors, i.e., $N_+ = N_-$; and (ii) Identical single motor parameters for plus and minus motors apart from their prefered directions. This latter feature implies the equalities

$$k_{\mathrm{off},+} = k_{\mathrm{off},-} \equiv k_{\mathrm{off}}, f_+ = f_- \equiv f \quad \text{and} \quad f_{\mathrm{s}} = 1 \tag{4.52}$$

for the desorption coefficients and force ratios and, thus, leads to a useful reduction in the number of parameters.

As one varies the force ratio $f$ and the desorption coefficient $k_{\mathrm{off}}$, the cargo particle exhibits three different motility states as shown in Fig. 22 for $N_+ = N_- = 4$: (i) 'No motion' states for small values of the force ratio $f$ corresponding to weak motors. In these states, the motor number distribution $P^{\mathrm{st}}(n_+, n_-)$ has a single maximum along the diagonal of the $(n_+, n_-)$-plane with $n_+ = n_-$ or $n_+ = n_- \pm 1$; (ii) Bi-directional transport states *without* pauses for large values of $f$ and desorption coefficients $k_{\mathrm{off}}$ that exceed a certain threshold value. The corresponding motor number distribution has two maxima of equal height at $(n_+, n_-) = (n, 0)$ and $(n_+, n_-) = (0, n)$; and (iii) Bi-directional transport states *with* pauses for relatively large values of $f$ and small values of $k_{\mathrm{off}}$. In this latter case, the distribution $P^{\mathrm{st}}(n_+, n_-)$ has three local maxima at $(n_+, n_-) = (n, 0)$, $(n_+, n_-) = (n', n')$, and $(n_+, n_-) = (0, n)$.

The different behavior of the three distinct motility regimes is illustrated in Fig. 23 for the three parameter values $(f, k_{\mathrm{off}})$ corresponding to the crosses A, B, and C in Fig. 22. State A with $(f, k_{\mathrm{off}}) = (2/3, 1/5)$ belongs to the 'no motion' regime, state B with $(f, k_{\mathrm{off}}) = (6/3, 1/5)$ to the regime of bi-directional transport without pauses, and state C with $(f, k_{\mathrm{off}}) = (4.75/3, 0.4/5)$ to the regime of bi-directional transport with pauses, see the three columns in Fig. 23. Each column contains the motor number distribution $P^{\mathrm{st}}(n_+, n_-)$, a typical trajectory of the cargo particle, and the distribution of instantaneous cargo velocities.

As shown in the left column of Fig. 23, the distribution $P^{\mathrm{st}}(n_+, n_-)$ for motility state A has a single maximum located at $(n_+, n_-) = (3, 3)$. This state exhibits no motion of the cargo apart from small fluctuations in both directions, and an instantaneous velocity distribution with a single peak at zero cargo velocity. In contrast, state B has a motor number distribution with two maxima at $(n_+, n_-) = (4, 0)$ and $(n_+, n_-) = (0, 4)$. In this state, the cargo performs fast directed motion both in the plus and in the minus direction but this motion does not exhibit any pauses. The latter property also follows from the velocity distribution, which is

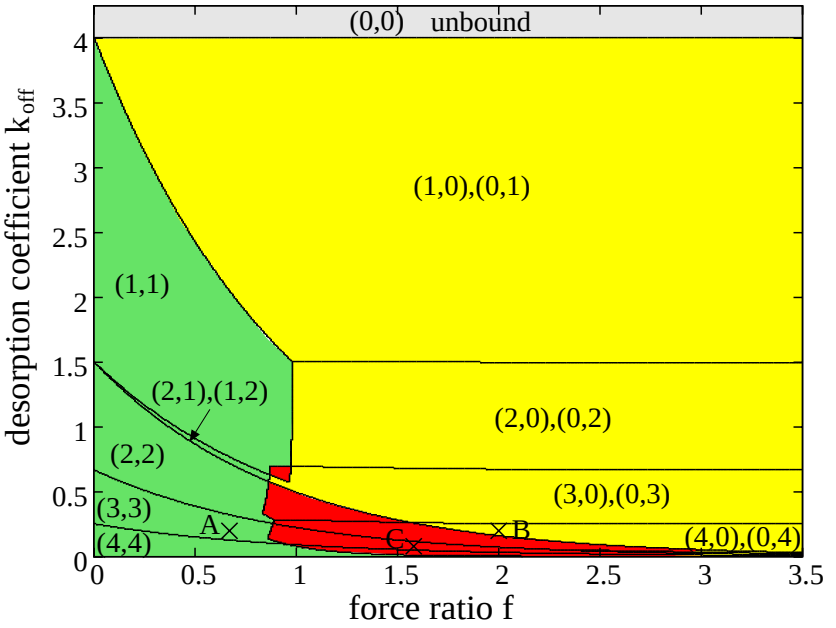


Fig. 22. Motility diagram for the symmetric tug-of-war of $N_+ = 4$ plus and $N_- = 4$ minus motors as a function of the force ratio $f$ and the desorption coefficient $k_{\rm off}$. Both motor species have identical single motor parameters apart from their prefered direction. Depending on the ratio $f = F_{\rm s}/F_{\rm d}$ of stall to detachment force and on the desorption coefficient $k_{\rm off} = \kappa_{\rm off}/\omega_{\rm on}$, the cargo particle exhibits three different types of motility states: (i) *'No motion' states* (green) for small values of the force ratio $f$. The motor number distribution $P^{\rm st}(n_+, n_-)$ has a single maximum located at $(n_+, n_-) = (n, n)$ or $(n_+, n_-) = (n, n\pm1)$. For sufficiently small values of the desorption coefficient $k_{\rm off}$, the number $n$ attains its maximal value $n = 4$ and decreases monotonically with increasing $k_{\rm off}$; (ii) *Bi-directional transport states without pauses* (yellow) for large values of $f$ and desorption coefficients $k_{\rm off}$ that exceed a certain threshold. The corresponding distribution $P^{\rm st}(n_+, n_-)$ has two maxima located at $(n_+, n_-) = (n, 0)$ and $(n_+, n_-) = (0, n)$; and (iii) *Bi-directional transport states with pauses* (red) for large $f$ and small $k_{\rm off}$. The three states labeled by A, B, and C are described in more detail in Fig. 23.[35]

bimodal with two peaks of equal height at $v_{\rm ca} = \pm1\,\mu$m/s. Finally, state C is characterized by a motor number distribution with three maxima at $(n_+, n_-) = (4, 0)$, $(n_+, n_-) = (3, 3)$, and $(n_+, n_-) = (0, 4)$. The cargo trajectories now exhibit fast motion in both directions as well as prolonged pauses leading to a velocity distribution with three peaks.

As one varies the motor numbers $N_+$ and $N_-$ with $N_+ = N_- \equiv N_1$, the qualitative features of the motility diagram and of the corresponding motility states of the cargo as illustrated in Fig. 22 and Fig. 23 for $N_1 = 4$ remain unchanged as has been shown in Ref. 85 by explicit simulations for $2 \leq N_1 \leq 10$.[m] As the motor number $N_1$ is increased, the distributions $P^{\rm st}(n_+, n_-)$ exhibit sharper and sharper maxima,

[m]The case $N_1 = 1$ is special since it does not exhibit any states corresponding to the regime of bi-directional transport with pauses.

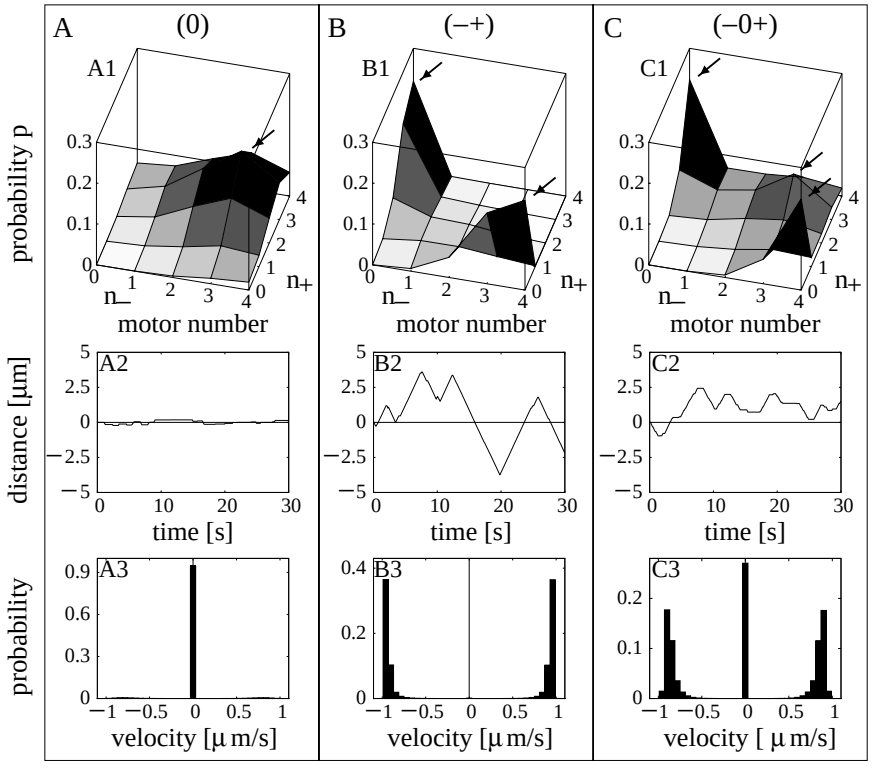


Fig. 23. Three motility states A, B, and C of a symmetric tug-of-war between $N_+ = 4$ plus and $N_- = 4$ minus motors corresponding to the three crosses in the motility diagram of Fig. 22: **(A)** *'No motion' state*: (A1) Motor number distribution $P^{\rm st}(n_+, n_-)$ with a single maximum at $(n_+, n_-) = (3, 3)$; (A2) Typical cargo trajectory with small excursions around the start position; and (A3) Distribution of instantaneous cargo velocities with a single peak at zero velocity. **(B)** *Bi-directional transport state without pauses*: (B1) Motor number distribution with two maxima at $(n_+, n_-) = (4, 0)$ and $(n_+, n_-) = (0, 4)$; (B2) Typical cargo trajectory with fast directed motion both in the plus and in the minus direction; and (B3) Velocity distribution with two peaks at cargo velocities $v_{\rm ca} = \pm 1\,\mu$m. **(C)** *Bi-directional transport state with pauses*: (C1) Motor number distribution with three maxima at $(n_+, n_-) = (4, 0)$, $(n_+, n_-) = (3, 3)$, and $(n_+, n_-) = (0, 4)$; (C2) Typical cargo trajectory with fast directed motion both in the plus and in the minus direction interupted by prolonged pauses; and (C3) Distribution of instantaneous cargo velocity with three peaks.[35]

and the switching times between these maxima increase exponentially with $N_1$ as has been numerically studied up to $N_1 = 80$ . This implies that the tug-of-war system leads to nonequilibrium phase transitions in the limit of large $N_1$.

## 5. Traffic of Motors and Cargo Particles

In this final section, we briefly review the traffic of motors and cargo particles that arises when many motors and/or cargo particles are bound to the filaments and the bound motors and particles start to bump into each other. Depending on their

interactions and on the compartment geometry, the motors can then form various spatio-temporal patterns such as traffic jams and undergo nonequilibrium phase transitions between different transport patterns.

### 5.1. *Overcrowding of filaments and traffic jams*

As mentioned before, single motors and cargo particles pulled by single motors ($N = 1$) behave as noninteracting particles if their molar concentrations belong to the dilute transport regimes as given by (3.15) and (3.17), respectively. The second relation, which involves the lateral size $\ell_{\rm ca}$ of the cargo particles, will also approximately apply to the more general case of cargo particles pulled by $N$ motors as long as the average step size of these cargo particles is of the order of $\ell$.

The dilute transport regime for single motors is given by $C \ll C_*$ with

$$C_* \equiv (\ell/\langle \Delta x \rangle) C_{\rm dis} \tag{5.1}$$

as follows from (3.15) for lateral motor size $\ell_{\rm mo} \simeq \ell$. For kinesin motors with step size $\ell = 8\,{\rm nm}$, average run length $\langle \Delta x \rangle = 1\,\mu{\rm m}$, and dissociation constant $C_{\rm dis} = 100\,{\rm nM}$, the crossover concentration $C_* \simeq 1\,{\rm nM}$. For motor concentrations $C > C_*$, the bound motors start to interact with each other, and these interactions become particularly strong when the filaments become overcrowded for concentrations $C \gtrsim C_{\rm dis}$ as follows from the definition (3.9) of the dissocation constant.

From the theoretical point of view, the overcrowding of filaments by motors should lead to traffic jams.[27] These jams are particularly pronounced in tube-like compartments that represent primitive models of axons.[27,37–39] Because of such traffic jams, the current or flux of the bound motors exhibits a maximum as one increases the total number of motors in the system. For a long tube-like compartment, e.g., the maximum is reached for half filling of the filament sites[37] corresponding to binding ratio $n_{\rm b} = 1/2$.[n] It is remarkable that the largest binding ratio reached by the kinesins as studied experimentally in Ref. 47, is about $n_{\rm b} = 1/2$. This seems to imply that these kinesin motors are able to avoid traffic jams in some way. As previously discussed in Ref. 7, several possible mechanisms for such a behavior can be envisaged: (i) The lateral size of stepping kinesins is increased compared to static kinesins; (ii) Stepping kinesins could increase their unbinding rate by bumping into each other; (iii) Stepping kinesins could reduce the binding rate for kinesin from the bulk solution, e.g., because of hydrodynamic interactions. Such a mechanism would imply that the effective binding rate decreases with increasing motor velocity; and (iv) The motors experience mutual interactions that lead to a certain preferred separation of the stepping kinesins. Further experiments seem to

[n]The half filling condition applies to simple motor walks as described in Sec. 3 provided the motors occupy a single filament site and $z \equiv \ell_{\rm mo}/\ell = 1$. If the motors occupy $z > 1$ binding sites, the maximum current is already reached for binding ratios $n_{\rm b} = 1/(z + \sqrt{z}) < 1/2$. On the other hand, if the motors occupy a single site but can dwell in two internal states, the maximum current is reached for binding ratios $n_{\rm b} > 1/2$ as shown in Ref. 70.

be necessary in order to clarify this issue. Jams of molecular motors have also been observed for other in vitro systems as described in Refs. 44–46.

Traffic jams are also expected to occur for the traffic of cargo particles. If the cargo particles are pulled by a single motor species, the cargo traffic is expected to be rather similar to the traffic of single motor molecules. For cargo particles pulled by two motor species, on the other hand, one would intuitively expect that jams can be reduced by bi-directional transport. Indeed, if a jam builds up in one direction, e.g., because of an obstacle, the cargo particles at the very end of the jam may then start to move in the opposite direction and, in this way, to dissolve the jam. This effect can be studied in more detail if one maps the bi-directional motion of many cargo particles onto lattice walks with both forward and backward steps, compare Fig. 12(c).

### 5.2. *Nonequilibrium phase transitions in motor traffic*

In our previous studies of motor traffic, we encountered several examples of nonequilibrium phase transitions.[37,38,48] Such transitions are interesting because a small change in a parameter leads to a huge response of the motor system and its transport properties.

The first examples for phase transitions in motor traffic were theoretically found for tube-like compartments with open orifices.[37] These transitions occur as one changes the boundary densities at these two orificies and are intimately related to the phase transitions found for asymmetric simple exclusion processes (ASEPs) in one dimension. The latter processes have been studied for a variety of systems, see, e.g., Refs. 61 and 86–91; an extensive review of ASEPs is contained in Ref. 92. In the last couple of years, several groups have also studied 1-dimensional ASEPs in contact with particle reservoirs,[93–95] which are closely related to the tube-like systems introduced in Refs. 27, 37.

A special kind of phase transition occurs in a half-open tube as shown in Fig. 24(a).[38] The left orifice is open, the right orifice is closed, a geometry that

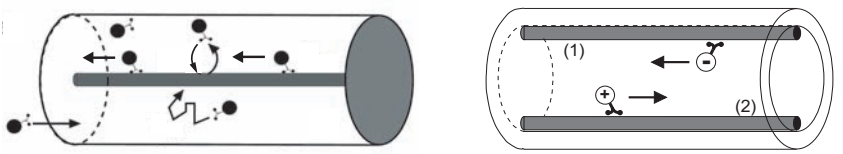


Fig. 24. Tube-like compartments that lead to nonequilibrium phase transitions in motor traffic: (a) Half-open tube with one motor species. When bound to the filament, the motors move towards the open orifice on the left. For small motor velocity, a jam builds up in front of this orifice. The jam length diverges in the limit of vanishing velocity or vanishing ATP concentration;[38] and (b) Tube with two motor species that walk into opposite directions and compete for the same binding sites on the filaments. This system undergoes a symmetry breaking phase transition, at which each filament becomes covered by either plus or minus motors.[48]

resembles the geometry of an axon. The closed orifice corresponds to the synaptic terminal whereas the motor reservoir at the open orifice corresponds to the cell body, where the motors are synthesized. Let us focus on the situation in which the tube contains only minus motors that would correspond to dynein motors in axons. The minus motors enter the tube by diffusing through the left orifice. Once they are bound to the filament, they walk back towards this orifice. As a result of this competition, the minus motors penetrate only up to a finite distance from the left orifice. As one decreases the velocity, e.g., by decreasing the ATP concentration and, thus, the chemical energy input $\Delta\mu$, this penetration increases and the minus motors form a traffic jam along the filament in front of the left orifice. This jam length diverges as $1/v$ for small $v$.[38] In these two examples of traffic phase transitions, the only interaction between the motors is provided by their mutual exclusion.

Another type of transition, that can be explored by varying the motor concentrations, occurs in systems with two species of motors that walk in opposite directions.[48] The simplest geometry is again provided by a tube-like compartment with periodic boundary conditions as shown in Fig. 24(b). Alternatively, one may consider systems with a constant density of unbound motors. As long as the motor-motor interactions are purely repulsive, the flux of bound motors is determined by the majority species, and the system evolves smoothly as one varies the motor concentrations. The situation becomes more interesting if one includes another, effectively attractive interaction between the bound motors as suggested by decoration experiments[96–99] in which filaments are decorated by motors and bare filament segments are observed to coexist with highly decorated segments. If the strength of this interaction is described by the paramter $q$, the system undergoes a traffic phase transition at a critical value $q = q_c$.[48] This phase transition occurs between two states with a spontaneously broken symmetry, for which one motor species is essentially excluded from the filaments. As one varies the bulk composition of the motors, the total motor flux develops a hysteresis loop across the phase boundary. In addition, if the system contains groups of isopolar filaments, the broken symmetry is directly visible via the coexistence of traffic lanes with opposite directionality as indicated in Fig. 24(b).

## 6. Summary and Outlook

In this article, we have reviewed recent work on the behavior of molecular motors that step along cytoskeletal filaments. Three motility regimes have been discussed in some detail: (i) Directed motion of single motors bound to the filaments in Sec. 2; (ii) Composite walks of these motors on length scales that are large compared to their run length in Sec. 3; and (iii) Cooperative transport by teams of molecular motors, which can lead to fast uni-directional or bi-directional motion in the Sec. 4. In addition, traffic jams and phase transitions in motor traffic have been briefly discussed in Sec. 5.

The general theoretical framework for the chemomechanical coupling of molecular motors, which determines the energy conversion by these motors, was summarized in Sec. 2. This framework is based on chemomechanical networks as shown in Fig. 5 and Fig. 7.[17,18] The network models for kinesin in Fig. 7 are able to describe all experimental data as obtained from single motor measurements.[19] In particular, they lead to a quantitative description of the motor velocity and run length as functions of load force, see Fig. 8 and Fig. 11, which determine the motor's stall and detachment force, respectively. For the 6-state model in Fig. 7(c), the stall force can be calculated explicitly as a function of chemical energy input and, thus, of ATP concentration, see relation (2.16). Another interesting set of quantities that has been calculated for this 6-state model is provided by the dwell time distributions for the mechanical steps as discussed in Sec. 2.3.6. These dwell times are difficult to measure with a high temporal resolution but the available data are again well described by this model without introducing any additional fit parameters.[20]

In Sec. 3, the reduced description of the motor molecule as a 'walker' has been discussed.[27,37,38] The motor undergoes composite walks consisting of directed (or biased) stepping when bound to the filament and diffusive (or random) walks in its unbound state away from the filament. The corresponding parameter mapping of the single motor parameters as discussed in Sec. 2 onto continuous-time and discrete-time walks is described in Sec. 3.2. The introduction of the motor's dissociation constant in (3.9) leads to a precise definition of the dilute transport regime as discussed in Sec. 3.2.2. In tube-like compartments as shown in Fig. 14(c) and (e), the effective transport velocity of the motor increases with the run length of the motor as follows from the explicit expression (3.27) for this velocity. When in contact with patterns of crossed filaments as in Fig. 16, the motors undergo active diffusion,[29] which is characterized by a strongly enhanced diffusion coefficient.

A single team of identical motors leads to uni-directional cargo transport as reviewed in Sec. 4.1. This cooperative transport mode has several advantages. First, the run length of the cargo particle is strongly increased with increasing motor number, see the explicit expression (4.9) and the comparison between theory and experiment in Fig. 18.[30,32] In the absence of additional forces, such an increased run length leads to a larger effective velocity of the cargo particle, compare (3.27), and to an increased diffusion constant for active diffusion as follows from the discussion in Sec. 3.5. Second, compared to a single motor, a team of $N$ motors can generate a larger force. This follows from the explicit expression (4.26) for the average cargo velocity in the presence of a load force. If a single motor has stall force $F_{\rm s}$, the team of $N$ identical motors has an apparent stall force that is of the order of $NF_{\rm s}$ for relatively small $N$ but substantially smaller than $NF_{\rm s}$ for large $N$.[30] Third, cooperative transport by $N$ motors offers additional possibilities for regulation. One example is provided by binding defects of the filaments such as tau proteins that reduce the rebinding rate of the detached motors.

In eukaryotic cells, vesicles and other cargo particles often carry both kinesins and dyneins, which leads to bi-directional transport along microtubules. The

observed transport behavior can be understood in terms of a stochastic tug-of-war[35] between the two motor teams as explained in Sec. 4.2. In order to define such a tug-of-war in a consistent manner, one has to take the instantaneous force balance between the two motor teams into account, see Sec. 4.2.3, which enters the transition rates between the different cargo states, see Sec. 4.2.4. The stochastic tug-of-war leads to rather complex transport behavior as observed experimentally. In general, one finds seven distinct motility regimes, which can be distinguished by the qualitative features of the motor number distribution $P^{\rm st}(n_+, n_-)$ as explained in Sec. 4.2.5. A particularly simple case is provided by a symmetric tug-of-war, see Sec. 4.2.6, because the symmetry reduces the number of possible motility states from seven to three. The corresponding motility diagram is shown in Fig. 22 and the motility behavior for the different regimes is illustrated in Fig. 23. The general, asymmetric case is discussed in Refs. 35 and 85.

The molecular motors considered here are found in all eukaryotic cells and provide the main machinery for force production and cargo transport in biological systems. On the one hand, we would like to obtain a systematic understanding of these biological processes. On the other hand, such an understanding is also necessary in order to construct useful biomimetic systems that are based on molecular motors. One example is provided by biomimetic transport systems that are inspired by the transport in axons since such systems represent promising alternatives to microfluidic devices, in which transport is coupled to flow induced by external pressure. Compared to pressure-induced flow, the transport by motors has several advantages such as: (i) Cargo transport is hardly affected by the viscosity of the aqueous solution and, thus, remains efficient even in a dense solution of macromolecules; (ii) Using two different motor species, different types of cargo can be simultaneously transported in both directions; and (iii) This transport system does not require rigid compartment walls but works in soft and flexible compartments as well. Another application of motors is their active diffusion, by which one can increase the diffusion constant of micrometer-sized cargo particles by several orders of magnitude as explained in Sec. 3.5. When integrated into existing biochips for DNA and RNA hybridization, these transport systems would act to increase the hybridization rates.

In general, active biomimetic systems based on molecular motors and filaments should have many applications in bioengineering, pharmocology and medicine. Such applications include sorting devices for biomolecules, motile drug delivery systems, molecular shuttles in 'labs-on-a-chip', and switchable scaffolds for tissue engineering. Thus, molecular motors and filaments are likely to become key components in the emerging soft nanotechnology.

## Acknowledgments

This work was supported by the EC sixth Framework Program (STREP Contract No. NMP4-CT-2004-516989).

**Glossary of Abbreviations and Symbols**

| | |
|---|---|
| $\alpha$ | probability for forward step of motor as in (3.19). |
| $A_{\rm cr}$ | cross-sectional area of tube. |
| ADP | adenosin diphosphate. |
| [ADP] | molar concentration of ADP. |
| ADP/P | product of ATP cleavage, abbreviated as $\Theta$. |
| ATP | adenosin triphosphate. |
| [ATP] | molar concentration of ATP. |
| $\beta$ | probability for backward step of motor as in (3.20). |
| $\mathcal{B}$ | backward cycle of single motor. |
| $c$ | mass density of motors in incubation chamber. |
| $c_o$ | mass density scale for motors as in (4.12). |
| $C$ | molar concentration of motor molecules around filament. |
| $C_{\rm dis}$ | dissociation constant for motor unbinding as in (3.9). |
| $C_{\rm eff}$ | effective motor concentration between cargo and filament. |
| $\mathcal{C}_\nu$ | cycle of network graph labeled by index $\nu$. |
| $\mathcal{C}_\nu^d$ | directed cycle or dicycle of network graph with direction $d$. |
| $d$ | direction of dicycle with $d = \pm$. |
| $d_\perp$ | dimensions perpendicular to filament; in practise, $d_\perp = 1$ or 2. |
| $\mathcal{D}$ | dissipative slip cycle of single motor. |
| $D_{\rm b}$ | diffusion constant for bound motor. |
| $D_{\rm ub}$ | diffusion constant of unbound motor. |
| $\Delta J_{ij}$ | local excess flux of transition $\|ij\rangle$ with $\Delta J_{ij} = J_{ij} - J_{ji}$. |
| $\Delta J(\mathcal{C}_\nu^d)$ | dicycle excess flux as in (2.10). |
| $\Delta J^{\rm st}(\mathcal{C}_\nu^d)$ | dicycle excess flux in steady state. |
| $\Delta\mu$ | chemical energy input from a single ATP hydrolysis as in (2.3) |
| $\Delta\mu(\mathcal{C}_\nu^d)$ | chemical energy change during dicycle $\mathcal{C}_\nu^d$. |
| $\Delta\bar{\mu}$ | reduced chemical energy input with $\Delta\bar{\mu} = \Delta\mu/k_BT$. |
| $\Delta t$ | run time of motor at filament. |
| $\langle\Delta t\rangle$ | average run time of motor. |
| $\Delta x$ | run length (or walking distance) of motor along filament. |
| $\langle\Delta x\rangle$ | average run length of motor. |
| $\epsilon_o$ | unbinding probability of single motor as in (3.18). |
| $F$ | load force acting on the motor; $F > 0$ for resisting load. |
| $F_{\rm d}$ | detachment force of single motor. |
| $F_{{\rm d},i}$ | detachment force for single motor in state $i$. |
| $F_{{\rm d},+}$ | detachment force of single plus motor. |
| $F_{{\rm d},-}$ | detachment force of single minus motor. |
| $F_{\rm s}$ | stall force of single motor. |
| $F_{{\rm s},+}$ | stall force of single plus motor. |
| $F_{{\rm s},-}$ | stall force of single minus motor. |
| $F_1$ | load force acting on a single motor. |

| | |
|---|---|
| $F_{1+}$ | load force acting on a single plus motor. |
| $F_{1-}$ | load force acting on a single minus motor. |
| $F_{n+}$ | load force acting on $n_+$ plus motors. |
| $F_{n-}$ | load force acting on $n_-$ minus motors. |
| $\mathcal{F}$ | forward cycle of single motor. |
| $\gamma$ | dwell probability of single motor as in (3.21). |
| $H_n$ | harmonic numbers as in (4.21). |
| $i$, $j$ | discrete states of a single motor bound to a filament. |
| $\|ij\rangle$ | transition or directed edge (di-edge) from state $i$ to state $j$. |
| $\langle ij\rangle$ | edge between states $i$ and $j$. |
| $J_{ij}$ | probability flux from motor state $i$ to state $j$ with $J_{ij} = P_i\omega_{ij}$. |
| $J(\mathcal{C}_\nu^d)$ | dicycle flux as in (2.11). |
| $J^{\mathrm{st}}(\mathcal{C}_\nu^d)$ | dicycle flux in steady state. |
| $k_{\mathrm{off}}$ | dimensionless desorption coefficient of motor as in (4.8). |
| $\kappa_{\mathrm{off}}$ | zero-force unbinding rate of motor as in (2.24). |
| $\kappa_{\mathrm{on}}$ | binding rate constant of motor as in (3.10). |
| $k_B$ | Boltzmann constant. |
| $K^{\mathrm{eq}}$ | equilibrium constant for ATP hydrolysis as in (2.4) and (2.5). |
| $\ell$ | step size of motor. |
| $\ell_{\mathrm{ca}}$ | number of filament sites occupied by cargo particle. |
| $\ell_{\mathrm{mo}}$ | number of filament sites occupied by single motor. |
| $\langle L_{\mathrm{b,b}}\rangle$ | average distance of bound motors. |
| $M$ | number of catalytic motor domains. |
| $\mu$ | chemical potential. |
| $\mu(X)$ | chemical potential for chemical species $X$ as in (2.2). |
| $n$ | number of identical motors that actively pull on a cargo particle. |
| $n_-$ | number of active minus motors with $0 \le n_- \le N_-$. |
| $n_+$ | number of active plus motors with $0 \le n_+ \le N_+$. |
| $(n)$ | state of cargo that is pulled by $n$ identical motors. |
| $n_{\mathrm{b}}$ | binding ratio as defined in (3.9). |
| $N$ | total number of motors attached to a single cargo particle. |
| $N_{\mathrm{Av}}$ | Avogadro's number. |
| $N_{\mathrm{b}}$ | number of motors bound to filament. |
| $N_{\mathrm{mo}}$ | total number of motors in the assay with $N_{\mathrm{mo}} = N_{\mathrm{b}} + N_{\mathrm{ub}}$. |
| $N_{\mathrm{si}}$ | total number of filament binding sites. |
| $N_{\mathrm{ub}}$ | number of unbound motors in the assay. |
| $N_-$ | total number of minus motors attached to a single cargo particle. |
| $N_+$ | total number of plus motors attached to a single cargo particle. |
| $N_1$ | number of one motor species for a symmetric tug-of-war. |
| $\mathcal{N}_{\mathrm{bea}}$ | number of beads included in run length statistics. |
| $(n_+, n_-)$ | state of cargo that is pulled by $n_+$ plus and $n_-$ motors. |
| $\nu$ | label for all cycles in the network. |

| | |
|---|---|
| $\omega_{ij}$ | transition rate for transition from motor state $i$ to state $j$. |
| $\omega_{n,n+1}$ | transition rate for transition from cargo state $(n)$ to state $(n+1)$. |
| $\omega_{\rm b}$ | transition rate for backward mechanical step as in (3.5). |
| $\omega_{\rm f}$ | transition rate for forward mechanical step as in (3.5). |
| $\omega_{\rm off}$ | force-dependent unbinding rate of motor as in (2.22). |
| $\omega_{\rm off,-}$ | unbinding rate of minus motor as in (4.31). |
| $\omega_{\rm off,+}$ | unbinding rate of plus motor as in (4.27). |
| $\omega_{\rm on}$ | concentration-dependent binding rate of motor as in (3.10). |
| $\omega_{\rm on,-}$ | binding rate of minus motor as in (4.32). |
| $\omega_{\rm on,+}$ | binding rate of plus motor as in (4.28). |
| P | inorganic phosphate. |
| $P_{\rm b}$ | probability that motor is bound to filament as in (3.26). |
| $P_i$ | probability that motor is in internal state $i$. |
| $P_i^{\rm st}$ | probability $P_i$ in steady state. |
| $P_{ij}(t)$ | probability for the motor to go from $i$ to $j$ during time $t$. |
| $P_{ij}^{\rm st}$ | probability for the motor to go from $i$ to $j$ for large $t$. |
| $P_n$ | probability that a cargo particle is in state $n$. |
| $\mathcal{P}_{\rm Ga}$ | Gaussian distribution. |
| $\mathcal{P}_{\rm Po}$ | Poisson distribution. |
| $\pi_o$ | binding probability for single filament site as in (3.24). |
| $\Pi_\omega(\mathcal{C}_\nu^d)$ | transition rate product along dicycle $\mathcal{C}_\nu^d$ as in (2.8). |
| $\Psi$ | average run length distribution of cargo as in (4.16). |
| $\Psi_N$ | run length distribution for cargo with $N$ motors. |
| $Q$ | reduced heat released by the motor. |
| $q$ | Sec. 2: ratio of forward to backward steps. |
| $q$ | Sec. 5: strength of attractive interaction between bound motors. |
| $\bar{Q}$ | reduced heat released by the motor with $\bar{Q} = Q/k_BT$. |
| $Q(\mathcal{C}_\nu^d)$ | heat released by the motor during completion of dicycle $\mathcal{C}_\nu^d$. |
| $\rho_{\rm b}$ | probability that filament site is occupied as in (3.13). |
| $\rho_{\rm ub}$ | volume fraction of motor heads as in (3.22). |
| $\rho_{\rm bf}$ | probability distribution for forward-after-backward steps as in (2.21). |
| $\rho_{\rm ff}$ | probability distribution for forward-after-forward steps as in (2.21). |
| $t$ | time. |
| $T$ | temperature. |
| $\tau_o$ | elementary time scale for discrete-time motor walks. |
| $\Theta$ | short-hand notation for ADP/P state of motor domain. |
| $v$ | average velocity of single motor in its bound state. |
| $V$ | volume. |
| $\mathcal{V}(F)$ | force-velocity relationship as in (4.24). |
| $\mathcal{V}_-(F)$ | force-velocity relationship for minus motors as in (4.33). |
| $\mathcal{V}_+(F)$ | force-velocity relationship for plus motors as in (4.29). |
| $v_{\rm ca}$ | average velocity of cargo particle in its bound state. |

| | |
|---|---|
| $v_{\mathrm{ca},n}$ | instantaneous velocity of cargo particle in cargo state $(n)$. |
| $v_{\mathrm{ca}}(n_+, n_-)$ | instantaneous velocity of cargo particle in cargo state $(n_+, n_-)$. |
| $W_{\mathrm{me}}$ | mechanical work performed by the motor. |
| $W_{\mathrm{me}}(\mathcal{C}_\nu)$ | mechanical work performed by the motor during dicycle $\mathcal{C}_\nu$. |
| $X$ | chemical species ATP, ADP or P. |
| $[X]$ | activity or molar concentration of chemical species $X$. |
| $[X]^*$ | activity scale for chemical species $X$ as given by (2.2). |

## References


1. B. Alberts, D. Bray, A. Johnson, J. Lewis, M. Raff, K. Roberts and P. Walter, *Essential Cell Biology: An Introduction to the Molecular Biology of the Cell*. Garland, New York, 1998.
2. D. Bray, *Cell Movements*. Garland Publ., New York, 2001.
3. J. Howard, *Mechanics of Motor Proteins and the Cytoskeleton*. Sinauer, New York, 1 edition, 2001.
4. M. Schliwa and G. Woehlke, Molecular motors, *Nature* **422**, 759–765 (2003).
5. R.D. Vale, The Molecular Motor Toolbox for Intracellular Transport, *Cell* **112**, 467–480 (2003).
6. R. Lipowsky and S. Klumpp, Life is Motion — Multiscale Motility of Molecular Motors, *Physica A* **352**, 53–112 (2005).
7. R. Lipowsky, Y. Chai, S. Klumpp, S. Liepelt and M. J. I. Müller, Molecular motor traffic: From biological nanomachines to macroscopic transport, *Physica A* **372**, 34–51 (2006).
8. K. Svoboda, Ch. F. Schmidt, B. J. Schnapp and St. M. Block, Direct observation of kinesin stepping by optical trapping interferometry, *Nature* **365**, 721–727 (1993).
9. A. Yildiz, M. Tomishige, R. D. Vale and P. R. Selvin, Kinesin walks hand–over–hand, *Science* **303**, 676–678 (2004).
10. N. J. Carter and R. A. Cross, Mechanics of the kinesin step, *Nature* **435**, 308–312 (2005).
11. M. J. Schnitzer and St. M. Block, Kinesin hydrolyses one ATP per 8–nm step, *Nature* **388**, 386–390 (1997).
12. D. D. Hackney, The tethered motor domain of a kinesin–microtubule complex catalyzes reversible synthesis of bound ATP, *PNAS* **102**, 18338–18343 (2005).
13. S. P. Gilbert, M. L. Moyer and K. A. Johnson, Alternating Site Mechanism of the Kinesin ATPase, *Biochemistry* **37**, 792–799 (1998).
14. L. Romberg and R. D. Vale, Chemomechanical cycle of kinesin differs from that of myosin, *Nature* **361**, 168–170 (1993).
15. I. Crevel, A. Lockhart and R. A. Cross, Weak and strong states of kinesin and ncd, *J. Mol. Biol.* **257**, 66–76 (1996).
16. N. R. Guydosh and S. M. Block, Backsteps induced by nucleotide analogs suggest the front head of kinesin is gated by strain, *Proc. Nat. Acad. Scie. USA* **103**, 8054–8059 (2006).
17. S. Liepelt and R. Lipowsky, Steady-state balance conditions for molecular motor cycles and stochastic nonequilibrium processes, *EPL*, 77:50002, 2007.
18. R. Lipowsky and S. Liepelt, Chemomechanical coupling of molecular motors: Thermodynamics, network representations, and balance conditions, *J. Stat. Phys.* **130**, 39–67 (2008).

19. S. Liepelt and R. Lipowsky, Kinesin's network of chemomechanical motor cycles, *Phys. Rev. Lett.* **98**, 258102 (2007).
20. A. Valleriani, S. Liepelt and R. Lipowsky, Dwell time distributions for kinesin's mechanical steps, *EPL* **82**, 28011 (2008).
21. K. Visscher, M. J. Schnitzer and S. M. Block, Single kinesin molecules studied with a molecular force clamp, *Nature* **400**, 184–189 (1999).
22. M. Nishiyama, H. Higuchi and T. Yanagida, Chemomechanical coupling of the forward and backward steps of single kinesin molecules, *Nature Cell Biol.* **4**, 790–797 (2002).
23. M. J. Schnitzer, K. Visscher and S. M. Block, Force production by single kinesin motors, *Nature Cell Biology* **2**, 718–723 (2000).
24. W. R. Schief, R.,H. Clark, A. H. Crevenna and J. Howard, Inhibition of kinesin motility by ADP and phosphate supports a hand–over–hand mechanism, *PNAS* **101**, 1183–1188 (2004).
25. S. M. Block, L. S. B. Goldstein and B. J. Schnapp, Bead movement by single kinesin molecules studied with optical tweezers, *Nature* **348**, 348–352 (1990).
26. A. Ajdari, Transport by active filaments, *Europhys. Lett.* **31**, 69–74 (1995).
27. R. Lipowsky, S. Klumpp and T. M. Nieuwenhuizen, Random walks of cytoskeletal motors in open and closed compartments, *Phys. Rev. Lett.* **87**, 108101 (2001).
28. T. M. Nieuwenhuizen, S. Klumpp and R. Lipowsky, Movements of molecular motors in two and three dimensions, *Europhys. Lett.* **58**, 468–474 (2002).
29. S. Klumpp and R. Lipowsky, Active diffusion of motor particles, *Phys. Rev. Lett.* **95**, 268102 (2005).
30. S. Klumpp and R. Lipowsky, Cooperative cargo transport by several molecular motors, *Proc. Nat. Acad. Sci. USA* **102**, 17284–17289 (2005).
31. M. Vershinin, B. C. Carter, D. S. Razafsky, S. J. King and S. P. Gross, Multiple-motor based transport and its regulation by Tau, *Proc. Nat. Acad. Sci. USA* **104**, 87–92 (2007).
32. J. Beeg, S. Klumpp, R. Dimova, R. S. Gracia, E. Unger and R. Lipowsky, Transport of beads by several kinesin motors, *Biophys. J.* **94**, 532–541 (2008).
33. S. P. Gross, Hither and yon: a review of bi–directional microtubule–based transport, *Phys. Biol.* **1**, R1–R11 (2004).
34. M. A. Welte, Bidirectional Transport along Microtubules, *Current Biology* **14**, R525–R537 (2004).
35. M. J. I. Müller, S. Klumpp and R. Lipowsky, Tug-of-war as a cooperative mechanism for bidirectional cargo transport by molecular motors, *Proc. Nat. Acad. Sci. USA* **105**, 4609–4614 (2008).
36. M. A. Welte and S. P. Gross, Molecular motors: a traffic cop within? *HFSP J.* **2**, 178–182 (2008).
37. S. Klumpp and R. Lipowsky, Traffic of molecular motors through open tube–like compartments, *J. Stat. Phys.* **113**, 233–268 (2003).
38. M. J. I. Müller, S. Klumpp and R. Lipowsky, Molecular motor traffic in a half-open tube, *J. Phys. Cond. Mat.* **17**, S3839–S3850 (2005).
39. S. Klumpp, M. J. I. Müller and R. Lipowsky, Traffic of Molecular Motors, in A. Schadschneider, T. Pöschel, R. Kühne, M. Schreckenberg and D. E. Wolf, editors, *Traffic and Granular Flow 05*, pages 251–261. Springer, Berlin, 2007.
40. D. D. Hurd and W. M. Saxton, Kinesin mutations cause motor neuron desease phenotypes by disrupting fast axonal transport in drosophila, *Genetics* **144**, 1075–1085 (1996).
41. M. A. Martin, S. J. Iyadurai, A. Gassman, Jr. J. G. Gindhart, T. S. Hays and W. M. Saxton, Cytoplasmic dynein, the dynactin complex, and kinesin are interdependent and essential for fast axonal transport, *Mol. Biol. Cell* **10**, 3717–3728 (1999).

42. S. Konzack, Funktion des Kinesin Motorproteins KipA bei der Organisation des Mikrotubuli–Cytoskeletts und beim polaren Wachstum von *Aspergillus nidulans*, doctoral thesis, University of Marburg (2004).
43. S. Konzack, P. E. Rischitor, C. Enke and R. Fischer, The role of the kinesin motor KipA in microtubule organization and polarized growth of Aspergillus nidulans, *Mol. Biol. Cell* **16**, 497–506 (2005).
44. I. M.-T. C. Crevel, M. Nyitrai, M. C. Alonso, S. Weiss, M. A. Geeves and R. A. Cross, What kinesin does at roadblocks: the coordination mechanism for molecular walking, *EMBO Journal* **23**, 23–32 (2004).
45. C. Leduc, O. Campas, K. B. Zeldovich, A. Roux, P. Jolimaitre, L. Bourel-Bonnet, B. Goud, J.-F. Joanny, P. Bassereau and J. Prost, Cooperative extraction of membrane nanotubes by molecular motors, *PNAS* **101**, 17096–17101 (2004).
46. K. Nishinari, Y. Okada, A. Schadschneider and D. Chowdhury, Intracellular Transport of Single–Headed Molecular Motors KIF1A, *Phys. Rev. Lett.* **95** 118101 (2005).
47. A. Seitz and T. Surrey, Processive movement of single kinesins on crowded microtubules visualized using quantum dots, *EMBO Journal* **25**, 267–277 (2006).
48. S. Klumpp and R. Lipowsky, Phase transitions in systems with two species of molecular motors, *Europhys. Lett.* **66**, 90–96 (2004).
49. P. Kraikivski, R. Lipowsky and J. Kierfeld, Enhanced Ordering of Interacting Filaments by Molecular Motors, *Phys. Rev. Lett.* **96**, 258103 (2006).
50. J. Kierfeld, P. Gutjahr, T. Kühne, P. Kraikivski and R. Lipowsky. Buckling, bundling, and pattern formation: From semi-flexible polymers to assemblies of interacting filaments, *J. Comp. Theo. Nanosci.* **3**, 898–911 (2006).
51. R. A. Alberty, Thermodynamics of the Hydrolysis of ATP as a Function of Temperature, pH, pMg, and Ionic Strength, *J. Phys. Chem. B* **107**, 12324–12330 (2003).
52. T. L. Hill, *Free Energy Transduction and Biochemical Cycle Kinetics*. Springer Verlag, New York, 1 edition, 1989.
53. A. Yildiz, J. N. Forkey, S. A. McKinney, T. Ha, Y. E. Goldmann and P. R. Selvin, Myosin V walks handover–hand: single fluorophore imaging with 1.5–nm localization, *Science* **300**, 2061–2065 (2003).
54. C. Veigel, F. Wang, M. L. Bartoo, J. R. Sellers and J. E. Molloy, The gated gait of the processive molecular motor, myosin V, *Nat. Cell Biol.* **4**, 59–65 (2002).
55. G. Cappello, P. Pierobon, C. Symonds, L. Busoni, J. Gebhardt, M. Rief and J. Prost, Myosin V stepping mechanism, *Proc. Nat. Acad. Sci. USA* **104**, 15328–15333 (2007).
56. R. Lipowsky, Universal aspects of the chemo–mechanical coupling for molecular motors, *Phys. Rev. Lett.* **85**, 4401–4404 (2000).
57. R. Lipowsky and N. Jaster, Molecular motor cycles: from ratchets to networks, *J. Stat. Phys.* **110**, 1141–1167 (2003).
58. U. Seifert, Entropy production along a stochastic trajectory and an integral fluctuation theorem, *Phys. Rev. Lett.* **95**, 040602 (2005).
59. D. J. Evans, E. G. D. Cohen and G. P. Morris, Probability of Second Law Violations in Shearing Steady States, *Phys. Rev. Lett.* **71**, 2401–2404 (1993).
60. G. E. Crooks, Entropy production fluctuation theorem and the nonequilibrium work relation for free energy differences, *Phys. Rev. E* **60**, 2721–2726 (1999).
61. J. L. Lebowitz and H. Spohn, A Gallavotti–Cohen–Type Symmetry in the Large Deviation Functional for Stochastic Dynamics, *J. Stat. Phys.* **95**, 333–365 (1999).
62. C. Jarzynski, Hamiltonian Derivation of a Detailed Fluctuation Theorem, *J. Stat. Phys.* **98**, 77–102 (2000).
63. S. Liepelt and R. Lipowsky, Operation modes of the molecular motor kinesin, *Phys. Rev. E (submitted)*, 2008.

64. St. J. King and T. A. Schroer, Dynactin increases the processivity of the cytoplasmic dynein motor, *Nat. Cell Biol.* **2**, 20–24 (2000).
65. A. D. Mehta, R. S. Rock, M. Rief, J. A. Spudich, M. S. Mooseker and R. E. Cheney, Myosin–V is a processive actin-based motor, *Nature* **400**, 590–593 (1999).
66. Z. Ökten, L. S. Churchman, R. S. Rock and J. A. Spudich, Myosin VI walks hand–over–hand along actin, *Nature Struct. Molecular Biol.* **11**, 884–887 (2004).
67. T. M. Nieuwenhuizen, S. Klumpp and R. Lipowsky, Random Walks of molecular motors arising from diffusional encounters with immobilized filaments, *Phys. Rev. E*, 69:061911, 2004.
68. S. Klumpp, T. M. Nieuwenhuizen and R. Lipowsky, Self-organized density patterns of molecular motors in arrays of cytoskeletal filaments, *Biophys. J.* **88**, 3118–3132 (2005).
69. T. M. Nieuwenhuizen, S. Klumpp and R. Lipowsky, Walks of molecular motors interacting with immobilized filaments, *Physica A* **350**, 122–130 (2005).
70. S. Klumpp, Y. Chai and R. Lipowsky, Effects of the chemomechanical stepping cycle on the traffic of molecular motors, *Phys. Rev. E* **78**, 041909 (2008).
71. D. C. Turner, C. Chang, K. Fang, S. L. Brandow and D. B. Murphy, Selective Adhesion of Functional Microtubules to Patterned Silane Surfaces, *Biophys. J.* **69**, 2782–2789 (1995).
72. H. Suzuki, A. Yamada, K. Oiwa, H. Nakayama and S. Mashiko, Control of Actin Moving Trajectory by Patterned Poly(methylmethacrylate) Tracks, *Biophys. J.* **72**, 1997–2001 (1997).
73. D. Riveline, A. Ott, F. Jülicher, D. A. Winkelmann, O. Cardoso, J.-J. Lacapere, S. Magnusdottir, J.-L. Viovy, L. Gorre-Talini and J. Prost, Acting on actin: the electric motility assay, *Eur. Biophys. J.* **27**, 403–408 (1998).
74. H. Hess, J. Clemmens, D. Qin, J. Howard and V. Vogel, Light–Controlled Molecular Shuttles Made from Motor Proteins Carrying Cargo on Engineered Surfaces, *Nano Lett.* **1**, 235–239 (2001).
75. Y. Hiratsuka, T. Tada, K. Oiwa, T. Kanayama and T. Q. P. Uyeda, Controlling the Direction of Kinesin–Driven Microtubule Movements along Microlithographic Tracks, *Biophys. J.* **81**, 1555–1561 (2001).
76. K. J. Böhm, R. Stracke, P. Mühling and E. Unger, Motor protein–driven unidirectional transport of micrometer–sized cargoes across isopolar microtubule arrays, *Nanotechnology* **12**, 238–244 (2001).
77. L. Limberis, J. J. Magda and R. J. Steward, Polarized Alignment and Surface Immobilization og Microtubules for Kinesin-Powered Nanodevices, *Nano Lett.* **1**, 277–280 (2001).
78. W. H. Roos, A. Roth, J. Konle, H. Presting, E. Sackmann and J. P. Spatz, Freely Suspended Actin Cortex Models on Arrays of Microfabricated Pillars, *Chem. Phys. Chem.* **4**, 872 (2003).
79. R. H. Miller and R. J. Lasek, Cross–bridges Mediate Anterograde and Retrograde Vesicle Transport along Microtubules in Squid Axoplasm, *J. Cell Biol.* **101**, 2181–2193 (1985).
80. A. Ashkin, K. Schütze, J. M. Dziedzic, U. Euteneuer and M. Schliwa, Force generation of organelle transport measured in vivo by an infrared laser trap, *Nature* **348**, 346–348 (1990).
81. S. P. Gross, M. A. Welte, S. M. Block and E. F. Wieschaus, Coordination of opposite–polarity microtubule motors, *J. Cell Biol.* **156**, 715–724 (2002).
82. D. B. Hill, M. J. Plaza, K. Bonin and G. Holzwarth, Fast vesicle transport in PC12 neurites: velocities and forces, *Eur. Biophys. J.* **33**, 623–632 (2004).

83. C. Kural, H. Kim, S. Syed, G. Goshima, V. I. Gelfand and P. R. Selvin, Kinesin and Dynein Move a Peroxisome in Vivo: A Tug–of–War or Coordinated Movement? *Science* **308**, 1469–1472 (2005).
84. V. Levi, A. S. Serpinskaya, E. Gratton and V. Gelfand, Organelle Transport along Microtubules in Xenopus Melanophores: Evidence for Cooperation between Multiple Motors, *Biophys. J.* **90**, 318–327 (2006).
85. M. J. I. Müller, S. Klumpp and R. Lipowsky, Motility states of molecular motors performing a tug-of-war, *J. Stat. Phys. (submitted)*, 2008.
86. C. T. MacDonald, J. H. Gibbs and A. C. Pipkin, Kinetics of biopolymerization on nucleic acid templates, *Biopolymers* **6**, 1–25 (1968).
87. F. Spitzer, Interaction of Markov Processes, *Adv. Math.* **5**, 246–290 (1970).
88. S. Katz, J. L. Lebowitz and H. Spohn, Nonequilibrium steady–states of stochastic lattice gas models of fast ionic conductors, *J. Stat. Phys.* **34**, 497–537 (1984).
89. J. Krug, Boundary–induced phase transitions in driven diffusive systems, *Phys. Rev. Lett.* **67**, 1882–1885 (1991).
90. A. B. Kolomeisky, G. M. Schütz, E. B. Kolomeisky and J. P. Straley, Phase diagram of one–dimensional driven lattice gases with open boundaries, *J. Phys. A: Math. Gen.* **31**, 6911–6919 (1998).
91. R. K. P. Zia, L. B. Shaw, B. Schmittmann and R. J. Astalos, Contrasts between equilibrium and nonequilibrium steady states: computer aided discoveries in simple lattice gases, *Computer Phys. Commun.* **127**, 23–31 (2000).
92. G.M. Schütz, Exactly solvable models for many–body systems far from equilibrium, in C. Domb and J. L. Lebowitz, editors, *Phase Transisions and Critical Phenomena*, volume 19, pages 3–251. Academic Press, London, 2001.
93. A. Parmeggiani, T. Franosch and E. Frey, Phase Coexistence in Driven One–Dimensional Transport, *Phys. Rev. Lett.* **90**, 086601/1–086601/4 (2003).
94. V. Popkov, A. Rakos, R. D. Willmann, A. B. Kolomeisky and G. M. Schütz, Localization of shocks in driven diffusive systems without particle number conservation, *Phys. Rev. E* **67**, 066117/1–066117/6 (2003).
95. M. R. Evans, R. Juhasz and L. Santen, Shock formation in an exclusion process with creation and annihilation, *Phys. Rev. E* **68**, 026117/1–066117/8 (2003).
96. D. T. Woodrum, S. A. Rich and T. D. Pollard, Evidence for biased bidirectional polymerization of actin filaments using heavy meromyosin prepared by an improved method, *J. Cell Biol.* **67**, 231–237 (1975).
97. A. Orlova and E. H. Egelman, Cooperative rigor binding of myosin to actin is a function of F–actin structure, *J. Mol. Biol.* **265**, 469–474 (1997).
98. A. Vilfan, E. Frey, F. Schwabl, M. Thormählen, Y.-H. Song and E. Mandelkow, Dynamics and Cooperativity of Microtubule, Decoration by the Motor Protein Kinesin, *J. Mol.Biol.* **312**, 1011–1026 (2001).
99. E. Muto, H. Sakai and K. Kaseda. Long-range cooperative binding of kinesin to a microtubule in the presence of ATP, *J. Cell Biol.* **168**, 691–696 (2005).